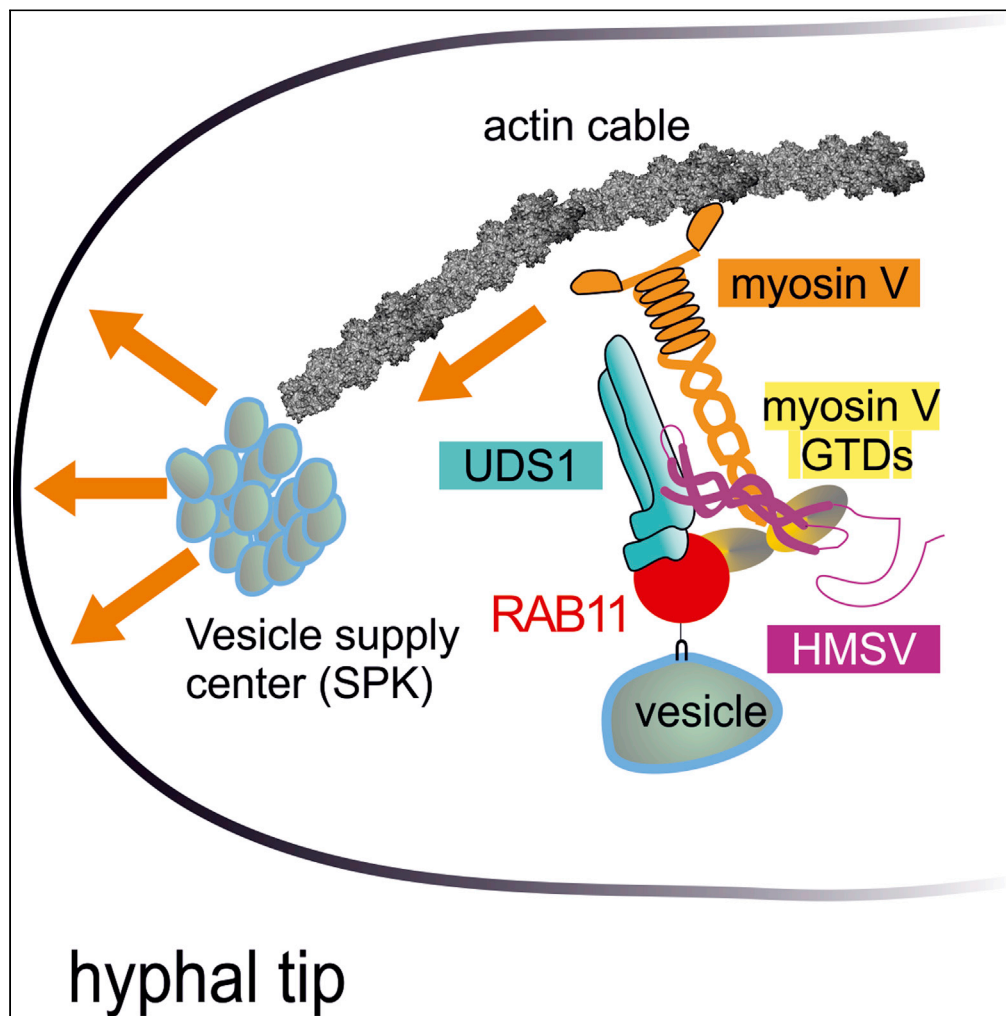


Article

The type V myosin-containing complex HUM is a RAB11 effector powering movement of secretory vesicles



Mario Pinar, Ana Alonso, Vivian de los Ríos, ..., Antonio Galindo, Ernesto Arias-Palomo, Miguel Á. Peñalva

penalva@cib.csic.es

Highlights

An apical exocytic organelle acting as vesicle supply center drives hyphal growth

Myosin V delivers RAB11 vesicles to this apical organelle, focusing exocytosis

RAB11 is the key organizer of the HUM complex recruiting myosin V to vesicles

Impairing HUM shifts myosin traffic to microtubules, defocusing secretory vesicles

Pinar et al., iScience 25, 104514
July 15, 2022 © 2022 The Authors.
<https://doi.org/10.1016/j.isci.2022.104514>

Article

The type V myosin-containing complex HUM is a RAB11 effector powering movement of secretory vesicles

Mario Pinar,^{1,5} Ana Alonso,¹ Vivian de los Ríos,² Ignacio Bravo-Plaza,¹ Álvaro de la Gandara,³ Antonio Galindo,⁴ Ernesto Arias-Palomo,³ and Miguel Á. Peñalva^{1,*}

SUMMARY

In the apex-directed RAB11 exocytic pathway of *Aspergillus nidulans*, kinesin-1/KinA conveys secretory vesicles (SVs) to the hyphal tip, where they are transferred to the type V myosin MyoE. MyoE concentrates SVs at an apical store located underneath the PM resembling the presynaptic active zone. A rod-shaped RAB11 effector, UDS1, and the intrinsically disordered and coiled-coil HMSV associate with MyoE in a stable HUM (HMSV-UDS1-MyoE) complex recruited by RAB11 to SVs through an interaction network involving RAB11 and HUM components, with the MyoE globular tail domain (GTD) binding both HMSV and RAB11-GTP and RAB11-GTP binding both the MyoE-GTD and UDS1. UDS1 bridges RAB11-GTP to HMSV, an avid interactor of the MyoE-GTD. The interaction between the UDS1-HMSV sub-complex and RAB11-GTP can be reconstituted *in vitro*. Ablating UDS1 or HMSV impairs actomyosin-mediated transport of SVs to the apex, resulting in spreading of RAB11 SVs across the apical dome as KinA/microtubule-dependent transport gains prominence.

INTRODUCTION

How the multiple functions of molecular motors are implemented within the crowded cytosol of a cell without causing an intracellular traffic jam constitutes a fundamental question of cell biology. Across the eukaryotic realm, type V myosins play a key role in the transport of membranous cargoes, often acting in concert with microtubule-dependent motors (Hammer and Sellers, 2012). For example, in the RAB11 pathway of the filamentous fungus *Aspergillus nidulans*, a single type V myosin (denoted MyoE) and a kinesin-1 (KinA) cooperate to transport RAB11 secretory vesicles (SVs) originating at the Golgi to the Spitzenkörper (SPK) (Pantazopoulou et al., 2014; Peñalva et al., 2017; Zhang et al., 2011). The SPK is a membraneless organelle adjacent to the apical plasma membrane (PM), characteristic of hyphal fungi. It acts as a vesicle supply center where SVs gather before being delivered to the growing tip's PM, with involvement of a second RAB GTPase, Sec4 (Riquelme et al., 2014; Steinberg et al., 2017). The SPK contains an F-actin organizing center (Sharpless and Harris, 2002), such that actin cables span the region of the tip spreading out from the apex like the ribs of an umbrella (Bergs et al., 2016; Pantazopoulou et al., 2014; Pearson et al., 2004; Taheri-Talesh et al., 2008). In contrast, microtubules (MTs) make contacts with their plus-ends at a broad, crescent-shaped region of the tip PM, which we denote here as "the apical dome."

A division of roles underlies cooperation between actomyosin and MT transport of *A. nidulans* RAB11 SVs (Pantazopoulou et al., 2014; Peñalva et al., 2017; Pinar et al., 2015; Pinar and Peñalva, 2020; Schuchardt et al., 2005; Zhang et al., 2011): KinA (kinesin-1) conveys RAB11 SVs to the hyphal tips, whereas MyoE concentrates them at the SPK (Figure 1A). The partially redundant role played by kinesin-1 makes MyoE nonessential, although its absence slows down growth markedly and causes morphological abnormalities resulting from inability to focus exocytosis at the apex. Cooperation between the microtubule and the actin cytoskeletons is not uncommon in tip-growing cells of organisms that are evolutionary distant from fungi. Another notable example of this cooperation occurs in the protonema of the moss *Physcomitrella patens*, which contains a cluster of F-actin at the apex that governs the directionality of growth and that strikingly resembles the fungal SPK/vesicle supply center (Wu and Bezanilla, 2018).

¹Department of Cellular and Molecular Biology, Centro de Investigaciones Biológicas CSIC, Ramiro de Maeztu 9, 28040 Madrid, Spain

²Proteomics Facility, Centro de Investigaciones Biológicas CSIC, Ramiro de Maeztu 9, 28040 Madrid, Spain

³Department of Chemical and Structural Biology, Centro de Investigaciones Biológicas CSIC, Ramiro de Maeztu 9, 28040 Madrid, Spain

⁴Division of Cell Biology, MRC Laboratory of Molecular Biology, Francis Crick Avenue, CB2 0QH Cambridge, UK

⁵Lead contact

*Correspondence: penalva@cib.csic.es
<https://doi.org/10.1016/j.isci.2022.104514>



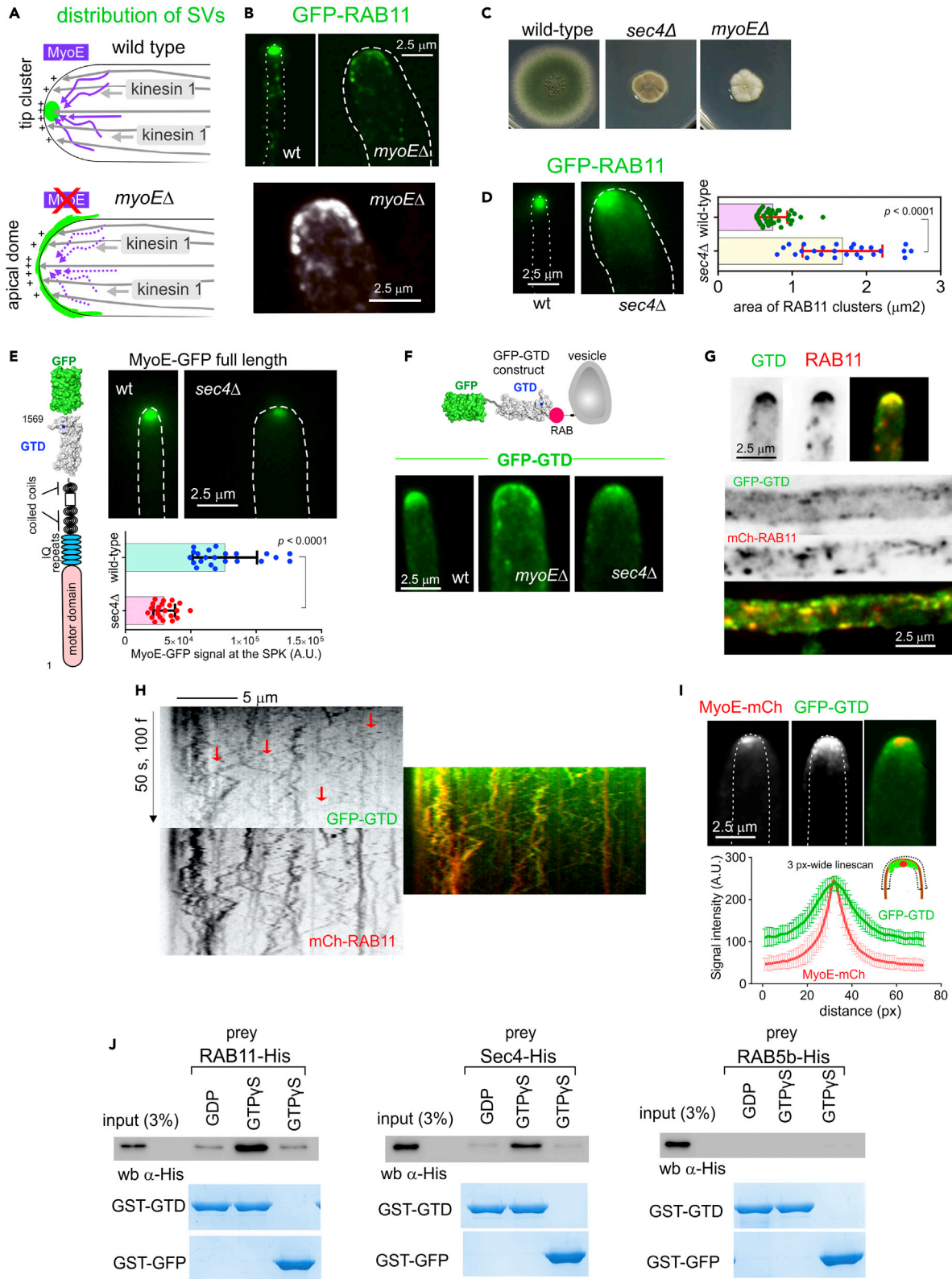


Figure 1. The type V myosin MyoE is a RAB11 effector

- (A) Schemes depicting cooperation of kinesin-1 (KinA) and MyoE to deliver RAB11 SVs to the SPK in the wild type and in a *myoEΔ* mutant in which SVs distribute across the apical dome, unable to be focused at the SPK due to the absence of F-actin-dependent transport.
- (B) (Top) Localization of GFP-RAB11 vesicles in a *myoEΔ* mutant. The picture is displayed with the same contrast adjustments as the wild-type. (Bottom) The image of *myoEΔ* has been magnified and contrasted to reveal the spreading of RAB11 SVs across the apical dome better.
- (C) Growth of indicated strains on solid complete medium at 37°C.
- (D) (Left) Localization of GFP-RAB11 vesicles in *sec4Δ* hyphae. The picture is displayed with the same contrast adjustments as the wild type. Right, quantitation of the area occupied by the apical cluster of RAB11 vesicles. The datasets were significantly different in a Mann-Whitney test ($p < 0.0001$). Bars indicate SD.
- (E) Localization of endogenously tagged MyoE-GFP in wild type and *sec4Δ* tips. The bottom graph shows that the MyoE-GFP signal at the SPK was significantly lower in *sec4Δ* cells compared with the wild type. The datasets were significantly different in a t student test with Welch's correction ($p < 0.0001$). Bars indicate SD.
- (F) Localization of GFP-tagged MyoE GTD in different genetic backgrounds. Unlike *myoEΔ* hyphae, wild type, and *sec4Δ* cells contain the resident copy of *myoE* intact.
- (G) GFP-GTD colocalizes with mCh-RAB11 in the tip cluster of SVs (top) and in cytosolic puncta (bottom).
- (H) Kymograph derived from a time-lapse movie built with near-cortical planes of a hypha co-expressing mCh-RAB11 and GFP-GTD. Tip-directed trajectories of SVs are indicated with arrows.
- (I) Dual-channel imaging of MyoE-mCh and GFP-MyoE GTD illustrating the larger area occupied by the latter. Graph, average results of linescans traced across the apical dome (scheme) ($n = 10$). Note the high cytosolic background of GFP-GTD.
- (J) GST pull-downs with GST-MyoE GTD as bait and the indicated bacterially expressed purified RABs, loaded with GDP or GTP γ S, as preys. GST-GFP was used as bait for a negative control. Pulled-down material was analyzed by α -His western blotting. The Coomassie-stained gel shows levels of GST fusion protein baits. See also [Figure S1A](#) and [Videos 1](#) through [4](#).

The key role that myosin-V-mediated transport plays in eukaryotic cells has prompted intensive research on the molecular mechanisms by which vesicles are recruited to the motor. Membranous cargoes attach to the globular C-terminal domain (GTD) of myosin V via "receptors" that are cargo-specific adaptors ([Hammer and Sellers, 2012](#); [Pashkova et al., 2006](#); [Wu et al., 2002](#)). In the case of SVs, these adaptors contain an RAB GTPase, be it RAB11, Sec4/RAB8, or both ([Wong and Weisman, 2021](#)). In *Saccharomyces cerevisiae*, Ypt31/32 (yeast RAB11s) and Sec4 (yeast Rab8) bind directly and without involvement of any other proteinaceous co-adaptor to the GTD of the type V myosin Myo2p ([Jin et al., 2011](#); [Lipatova et al., 2008](#); [Santiago-Tirado et al., 2011](#)), with additional involvement of PtdIns4P present in SVs in their association with the motor ([Santiago-Tirado et al., 2011](#)). However, in the particular case of RAB11, this paradigm of the RAB as the only component of the myosin V adaptor to vesicles is far from being universal. For example, in mammalian cells the RAB11a effector RAB11-FIP2 (RAB11 family interacting protein 2) acts as co-adaptor cooperating with the GTPase to recruit MyoVb to recycling endosome vesicles ([Hales et al., 2002](#); [Schafer et al., 2014](#); [Wang et al., 2008](#)), the actin nucleator SPIR-2 acts as co-adaptor between RAB11 and MyoVa ([Pylypenko et al., 2016](#)) and in flies dRip11 acts as co-adaptor of RAB11 to recruit myosin V to exocytic vesicles and deliver them to the rhabdome base ([Li et al., 2007](#)). Perhaps reflecting that, to our knowledge, RAB11 might be unable to interact with more than two effectors simultaneously ([Burke et al., 2014](#); [Vetter et al., 2015](#)), RAB11-based myosin V adaptor complexes of greater complexity have not been reported.

Intracellular distances in hyphal tip cells are remarkably large (up to 125 μm from tip to septum). Thus, it is unsurprising that *A. nidulans* uses MTs for the long-distance shuttling of membranous organelles. This feature has been experimentally advantageous to study adaptors by which organelles engage motors. For example, studies on the MT-dependent movement of early endosomes in *A. nidulans* led to the discovery of the FTS/Hook/FHIP (FHF) complex serving as adaptor between dynein and endosome cargo ([Bielska et al., 2014](#); [Qiu et al., 2019](#); [Yao et al., 2014](#); [Zhang et al., 2014](#)). Hyphae of *A. nidulans* grow by apical extension at $\sim 1 \mu\text{m}/\text{min}$ at 28°C, implying that transport of SVs to the extending tip is optimized to meet the high demand of lipids that fuel the expansion in membrane surface, as well as to deliver enzymes that modify the cell wall to facilitate growth. SVs are loaded with three motors: myosin V, kinesin-1, and dynein ([Peñalva et al., 2017](#)). It has been suggested that SVs are handed over from kinesin-1 to myosin V in the region of the tip, hypothetically by switching from MT to actin cables, yet the mechanism by which myosin V prevails over kinesin-1 in the tip region is not understood. In view of the crucial role that myosin V plays in the lifestyle of hyphal fungi, we hypothesized that accessory proteins might help this motor to engage RAB11 SVs robustly, to ensure the efficiency of the latest step in their transport. Here we report the molecular composition of a novel myosin-V-containing complex that engages SVs. This complex, denoted HUM, also contains UDS1 and HMSV, two proteins whose orthologues in *Neurospora crassa* have been recently identified as components of the SPK ([Zheng et al., 2020](#)). Trafficking of RAB11 SVs to the SPK/vesicle supply center is impaired if the HUM complex is disrupted.

RESULTS

MyoE is key for the delivery of RAB11 secretory vesicles to the hyphal apex

The efficiency of MyoE transport is reflected in the distribution of RAB11 SVs accumulating in the tips before fusing with the PM. Although in the wild type these SVs gather at the SPK and its environs, in *myoEΔ* cells lacking type V myosin SVs cannot be focused at the apex, yet they still arrive at the tip by kinesin-1/microtubule-mediated transport (Pantazopoulou et al., 2014; Peñalva et al., 2017) (Figures 1A and 1B); this results in relocation of RAB11 vesicles to a tip crescent whose shape reflects the steady-state distribution of the microtubules' plus-ends contacting the apical dome cortex (Figure 1A). *myoEΔ*-dependent delocalization of RAB11 to this crescent is paralleled by a conspicuous reduction of RAB11 in the tip (Figure 1B), strongly suggesting that MyoE is a major contributor to the transport of RAB11. Consistent with a secretory defect, loss of MyoE markedly reduces growth (Figure 1C) and alters hyphal morphogenesis, leading to abnormally wide cells (Figures 1B and 1F; note that exocytosis determines the shape of the cell wall) (Hernández-González et al., 2014, 2018a; Pinar et al., 2013a, 2013b).

In budding yeast, the RAB GTPase Sec4 (metazoan RAB8) acts downstream of RAB11 during transport between the *trans*-Golgi network (TGN) and the PM and ultimately mediates fusion of SVs with the membrane (Donovan and Bretscher, 2015a; 2015b; Jin et al., 2011; Santiago-Tirado et al., 2011). In *A. nidulans* Sec4 localizes to the hyphal tips, which suggests a similar role. Therefore, Sec4 was an obvious candidate to adapt MyoE to SVs; this could be tested directly because Sec4 is not essential in *A. nidulans*, although its absence is as debilitating as that of MyoE (Figure 1C). However, contrasting to *myoEΔ* mutants, *sec4Δ* mutants are still capable of gathering RAB11 SVs at the tip (Figure 1D), indicating that Sec4 is not essential for transport. Instead, we observed that the cluster of SVs accumulating in *sec4Δ* tips was twice as broad as in the wild type (1.68 ± 0.5 SD versus $0.74 \pm 0.2 \mu\text{m}^2$, $p=0.0001$ in a Mann-Whitney t test), while still displaying a similar average intensity per pixel, which suggests that the number of vesicles accumulating in the mutant was consistently higher than the wild type (Puermer et al., 2021). This cluster of RAB11 SVs at the tip, less tightly packed in the *sec4Δ* mutant than in the wild type, appears to be submitted to the opposing forces exerted by anterograde and retrograde motor teams, often causing the detachment of RAB11 SV 'lumps' away from the apex (Video S1). Therefore, all these data suggest that rather than mediating the myosin V-mediated delivery of SVs to the tip, the main role of Sec4 is participating in the consumption of SVs. Yet, Sec4 detectably contributes to transport, as although *sec4Δ* cells still concentrated MyoE at the SPK, they did so with lesser efficiency than the wild type (Figure 1E and Video S2; note that MyoE is activated by cargo loading). Altogether, these data established that there must be another adaptor sharing with Sec4 the task of engaging SVs to MyoE.

Both RAB11 and Sec4 interact directly with MyoE

Previous studies with fungal and metazoan cells pointed to RAB11 as the most likely candidate (Goldenberg, 2015; Hales et al., 2002; Lipatova et al., 2008; Roland et al., 2011). In the intensively studied transport of SVs to the growing bud of *S. cerevisiae*, the RAB11 homologues Ypt31/32 and Sec4 recruit the MyoE orthologue Myo2p through direct binding to the highly conserved globular tail domain (GTD) of the latter (Jin et al., 2011; Lipatova et al., 2008). If this mechanism were conserved in *A. nidulans*, a polypeptide consisting solely of the MyoE GTD domain should bind the RABs present on SVs, being passively transported along with them to the tips. To test this prediction, we expressed a construct consisting of the GFP-tagged MyoE GTD domain in wild type, *myoEΔ* and *sec4Δ* hyphae. In the wild type, GFP-GTD, although cytosolic in part, concentrated at a tip cluster (Figure 1F), on which it strictly colocalized with RAB11, and to punctate structures barely noticeable over the cytosolic background (Figures 1F and 1G). The low signal-to-background ratio and the rapid movement of some of these cytosolic structures made colocalization studies with RAB11 challenging, but we managed to obtain informative time-lapse sequences with a temporal resolution of 2 fps using a beam splitter to film the two channels simultaneously, coupled to a CMOS camera that allowed us to set different acquisition times for each channel to compensate differences in brightness. These experiments showed that GFP-GTD puncta were RAB11 positive (Figures 1G and 1H and Video S3). This key *in vivo* observation strongly suggested that the GTD is indeed sufficient to localize to RAB11-containing SVs powered by resident KinA and MyoE. Figure 1I shows that the region at which GFP-GTD localizes is broader than the apical spot at which full-length MyoE-mCherry does, suggesting that the localization of GFP-GTD cannot be the result of an interaction of the GFP-GTD fusion protein with resident MyoE. Indeed, in *myoEΔ* cells GFP-GTD localized to the apical dome, recapitulating the distribution of RAB11 SVs in this mutant (Figures 1B and 1F) (Video S4) and indicating that GFP-GTD can still ride on SVs when MyoE is absent. The observation that MyoE GTD still concentrated at the apex of *sec4Δ* cells (Figure 1F)

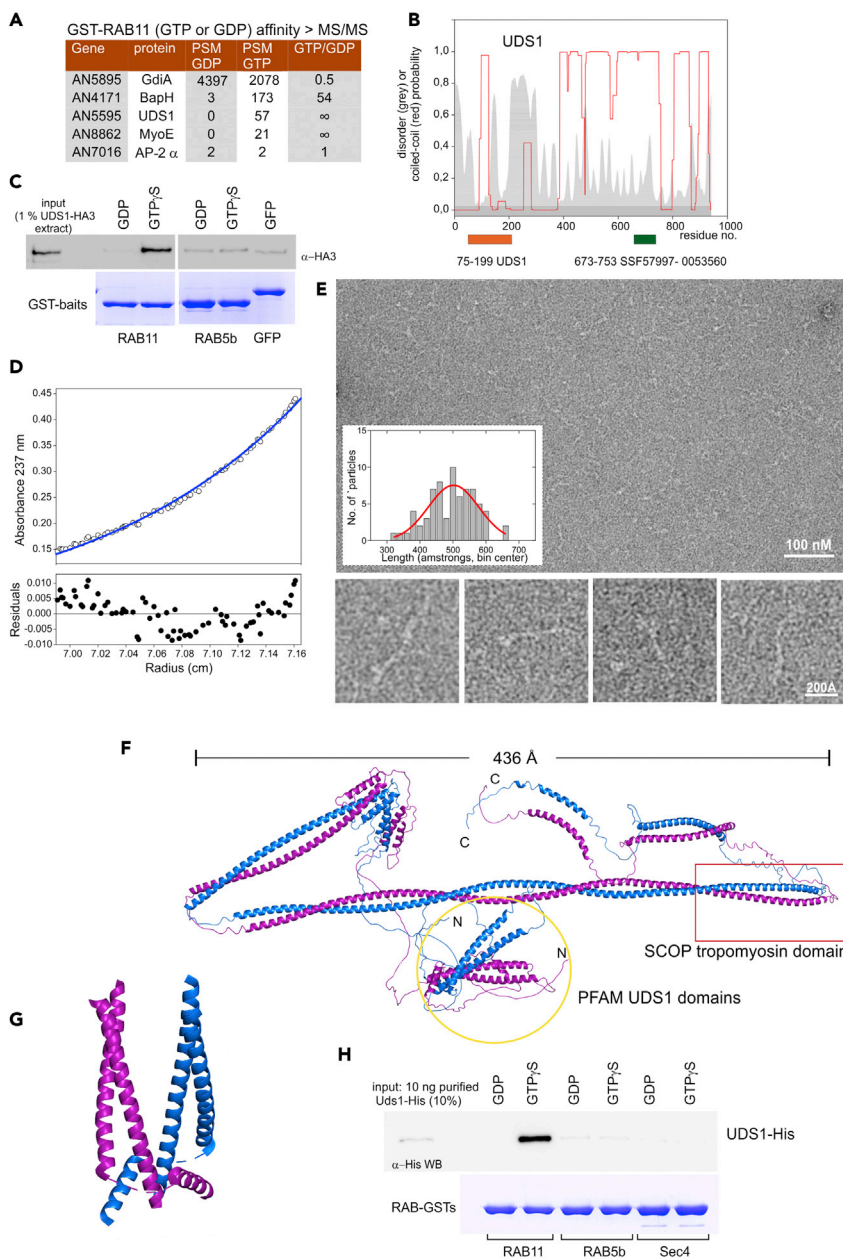


Figure 2. UDS1, a novel, direct effector of RAB11

(A) Proteins retained by GTP γ S- and GDP-loaded RAB11-GST columns were identified by shotgun proteomics. Spectral counts obtained for each protein and condition and the relative enrichment detected in one sample versus the other are listed. Note that markedly abundant GdiA (GDP dissociation factor) interacts preferentially with GDP-RAB11. AP-2 α was used as negative control.

(B) Features of UDS1. The probability of forming coiled-coils (red graph) and disordered regions (gray area) is indicated, as are the positions of the UDS1 and SCOP superfamily domains.

(C) GST pull-down assays with the indicated baits, using a prey extract of *A. nidulans*-expressing UDS1-HA3 from the endogenously tagged gene. Pull-downs were analyzed by western blotting with α -HA3 antibody. GST-GFP was used as negative bait control.

(D) UDS1 is a dimer *in vitro*. Equilibrium ultracentrifugation of purified UDS1 at a concentration of 4 μ M; (top) the concentration gradient obtained (empty circles) is shown together with the best-fit analysis assuming that the protein is a dimer. (Bottom plot) Differences between experimental data and estimated values for the dimer model (residuals). See also Figure S2E Negative-stain electron microscopy of purified UDS1. The proteins were stained with uranyl acetate and

Figure 2. Continued

examined in a JEOL-1230 electron microscope. Four examples selected showed the extended screw-like form of UDS1. The lengths of $N = 71$ molecules were measured (plot; average $496 \text{ \AA} \pm 73 \text{ SD}$).

(F) AlphaFold prediction of the UDS1 dimer. See [Figures S3A and S3B](#).

(G) Enlarged view of the predicted fold of the UDS1 domain dimer.

(H) GST pull-down assays with the indicated RABs and purified UDS1-His as prey. UDS1 was detected by α -His western blotting.

strongly indicated that Sec4 cannot be an exclusive receptor for MyoE. Thus, we concluded that the MyoE GTD is sufficient to engage the motor to at least two receptors present on SVs, with the obvious candidates being Sec4 and RAB11.

In view of this conclusion, we asked whether the type V myosin MyoE is a direct effector of these RABs. We purified His-tagged versions of Sec4, RAB11, and, as control, Rab5b acting in the endocytic pathway ([Abenza et al., 2010](#)). These RABs were loaded with GDP or GTP γ S and used as preys in pull-down assays with MyoE GST-GTD or GST-GFP baits (GFP, known to be sticky, was used as negative control). Bound proteins were resolved by electrophoresis, and RABs retained by the baits were detected by western blotting, after reacting the membranes with α -His antibody. Both GTP γ S-loaded RAB11 and Sec4 were captured by the GTD, but not by the GFP bait, whereas RAB11-GDP, Sec4-GDP, and Rab5b (whether GDP or GTP γ S) were not ([Figure 1J](#)). Thus, Sec4 and RAB11 bind the MyoE GTD directly, specifically, and in nucleotide switch-dependent manner.

A double mutant in which *sec4* Δ was combined with *hypA1ts*, a mutation affecting the RAB11 GEF TRAPP11 ([Pinar et al., 2015](#)), is virtually lethal ([Figure S1A](#)); this is consistent with the involvement of both Sec4 and RAB11 in exocytosis. However, the fact that *sec4* Δ can accumulate vesicles in the apical region ([Figure 1D](#)) indicates that, of these two RABs, RAB11 is by itself sufficient to mediate the MyoE-mediated clustering of SVs at the vesicle supply center.

The actomyosin pathway protein UDS1 is a novel RAB11 effector

As we were most interested in the effectors of RAB11, we investigated if, similar to the situation with mammalian RAB11 and myosin Vb ([Hales et al., 2002](#); [Schafer et al., 2014](#)), other associates cooperate with RAB11 in the transport of secretory vesicles. We identified by liquid chromatography and tandem mass spectrometry (LC-MS/MS) the proteins retained by glutathione Sepharose beads containing RAB11-GST baits loaded with GDP or GTP γ S. The resulting hits were ordered by abundance of peptide spectral matches (PSMs) in the GTP γ S sample relative to the GDP one, which helped to identify potential physiological hits. The highly abundant GDP-dissociation inhibitor GdiA ([Pinar et al., 2015](#)) served as specific GDP-RAB binder control, the previously characterized and abundant RAB11-GTP effector BapH ([Pinar and Peñalva, 2017](#)) served as positive control, and the unrelated AP-2 alpha-adaptin as negative one ([Figure 2A](#)). This analysis highlighted two potential actin-related hits. One was MyoE itself, which was exclusively retained by GTP-loaded, but not by GDP-loaded, GST-RAB11 beads, reinforcing the conclusion that MyoE is a RAB11 effector. The second was the relatively abundant and highly specific RAB11-GTP effector AN5595 ([Figure 2A](#)). The 941 residue AN5595 product has a strong tendency to form coiled-coils ([Figure 2B](#)). An *N. crassa* orthologue of AN5595 denoted JANUS-1 interacts with the polarisome component Spa2 and has been suggested to serve as an SPK scaffold ([Zheng et al., 2020](#)), yet *A. nidulans* Spa2 is not required for the establishment or maintenance of the SPK, nor for the localization of formin ([Virag and Harris, 2006](#)). However, AN5595 shows features of an actomyosin regulator ([Figure 2B](#)), as it contains a SCOP superfamily tropomyosin domain (SSF57997) suggestive of a parallel coiled-coil quaternary structure, and a UDS1 domain (PF15456). This domain was named after the as-yet uncharacterized AN5595 *Schizosaccharomyces pombe* homologue, whose name stands for “upregulated during septation,” and which localizes to the contractile actin ring in the fission yeast mitotic septum ([Ikebe et al., 2011](#)). Therefore, we denoted AN5595 as UDS1.

To confirm that UDS1 is a *bona fide* RAB11 effector, we HA3-tagged the protein endogenously and used UDS1-HA3 cell extracts in pull-down assays with purified GST-RAB baits, loaded with GTP γ S or GDP, and with GST-GFP as negative control. UDS1-HA3 was pulled down solely by GTP γ S-RAB11 but not by GFP, GDP-RAB11, GTP γ S-RAB5b, or GDP-RAB5b baits ([Figure 2C](#)), confirming that UDS1 is subordinated to RAB11.

Next, we purified UDS1-His6 from bacteria. By gel filtration chromatography UDS1 eluted at a position corresponding to >600 kDa (Figure S2), suggesting homo-oligomerization and/or a 3D structure substantially deviating from the globular shape. Sedimentation equilibrium ultracentrifugation of purified UDS1 (Mr 106,857 Da) revealed a buoyant mass of $57,002 \pm 403$ Da corresponding to a molar mass of $209,073\text{Da} \pm 1,612$ Da, matching the molecular weight of a dimer (Figure 2D). Moreover, although the flexibility observed at the level of individual particles precluded us from obtaining 2D averages, individual EM images revealed that UDS1 presents a rod-shaped structure highly suggestive of an elongated coiled-coiled dimer, with an approximate length of ~ 500 Å (Figure 2E).

We used AlphaFold to gain insight into the architecture of UDS1, after imposing the restriction that the protein is a dimer. We obtained a structure that has notable resemblance to some of the EM pictures (Figures 2E and 2F; Figures S3A and S3B). The structure contains a 436 Å-long parallel coiled-coil, which fits reasonably well with the experimentally determined length of ~ 500 Å for the complete protein (Figure 2E histogram). This section of the protein, which is predicted with good pDLLT (per residue-estimate of confidence) values (Figure S3A), contains on its C-terminal side the SCOP tropomyosin domain. The V-shaped UDS1 domain is composed of two adjacent tri-helical units, with the two longest helices forming the two arms of the V (Figure 2G).

Lastly, as the above RAB pull-down experiments using cell extracts do not rule out the possibility that RAB11 and UDS1 interact by way of bridging protein(s), we used His-tagged UDS1 to repeat the GST-RAB pull-down assays with purified proteins. Figure 2H shows that UDS1-His behaves as the protein present in *Aspergillus* extracts, being pulled down by GTP γ S-RAB11 but not by GDP-RAB11, nor by the inactive or active forms of RAB5b and Sec4. In summary, UDS1 is a coiled-coil dimer that binds directly to the (GTP) active form of RAB11. Importantly, UDS1 does not bind to Sec4, the other MyoE receptor present on SVs.

***Aspergillus* UDS1 colocalizes with both MyoE and RAB11 on SVs**

In current models (Figure 1A), RAB11 SVs arrive at the tip using KinA (kinesin-1) and are concentrated at the SPK by MyoE. Figure 3A shows that in agreement with these models RAB11 SVs fill a region at the tip that is broader than the SPK, as defined by the MyoE-GFP signal. In colocalization experiments with RAB11, UDS1 behaves like MyoE, being restricted to the SPK (Figure 3B and Video S5). The slightly broader distribution of RAB11 SVs at the tip region reflects that SVs can arrive at the tip transported by KinA, in addition to MyoE (Figures 1A, 3A and 3B). The behavior of UDS1, akin to that of MyoE, is consistent with UDS1 being a MyoE associate. Indeed, as predicted, UDS1 strictly colocalizes with myosin V in still images (Figure 3C) and across time, as seen in Figure 3D kymograph (derived from Video S6) covering >15 min of hyphal growth. Notably, in the absence of MyoE, which results in delocalization of RAB11 vesicles from the SPK to the apical dome (Figure 1B), UDS1 strictly colocalizes with RAB11 SVs delivered to the apical dome by MTs (Figure 3E), which strongly supports the notion that UDS1 travels with SVs rather than being a permanent resident of the SPK. Indeed, Video S7 shows how UDS1-GFP recurs in the apical dome of a *myoE* Δ tip as SVs containing UDS1 arrive by MT transport to the PM. Thus, UDS1 is a RAB11 effector that is present in SVs and concentrates at the SPK.

MyoE associates directly with HMSV, a further novel component of the RAB11 pathway

To investigate the possibility that MyoE and UDS1 associate, we analyzed, by LC-MS/MS, GFP-Trap immunoprecipitates of MyoE-GFP and UDS1-GFP cell extracts, using immunoprecipitates of a strain expressing the unrelated bait *Uso1*-GFP as a negative control (*Uso1*/p115 acts as a tether in the ER/Golgi interface). UDS1 indeed pulled down MyoE, whereas MyoE pulled down UDS1 inefficiently, suggestive of weak or indirect interaction (Figure 4A). Remarkably, an as-yet uncharacterized protein, the product of AN1213, coprecipitated with MyoE-GFP quite efficiently. Conversely, MyoE coprecipitated efficiently with GFP-tagged AN1213. An orthologue of AN1213, denoted SPZ-1, has been investigated in *N. crassa* and proposed to serve as scaffold at the SPK (Zheng et al., 2020). However, for reasons that become clear below we denoted AN1213 as HMSV (hooking myosin to SVs). HMSV coprecipitated with UDS1-GFP as well, indicating that these proteins also interact (Figure 4A). Notably, the polarisome component SpaA/Spa2, which has been shown to associate with *N. crassa* SPZ-1, JANUS-1, and myosin V (Zheng et al., 2020), does not immunoprecipitate with the *A. nidulans* orthologues (Figure 4A) (see discussion).

HMSV is a 994 residue-long protein whose 350 N-terminal residues are predicted by COIL to be disordered, whereas the remaining ~ 650 residues have strong propensity to form coiled-coils (Figure 4B). We used

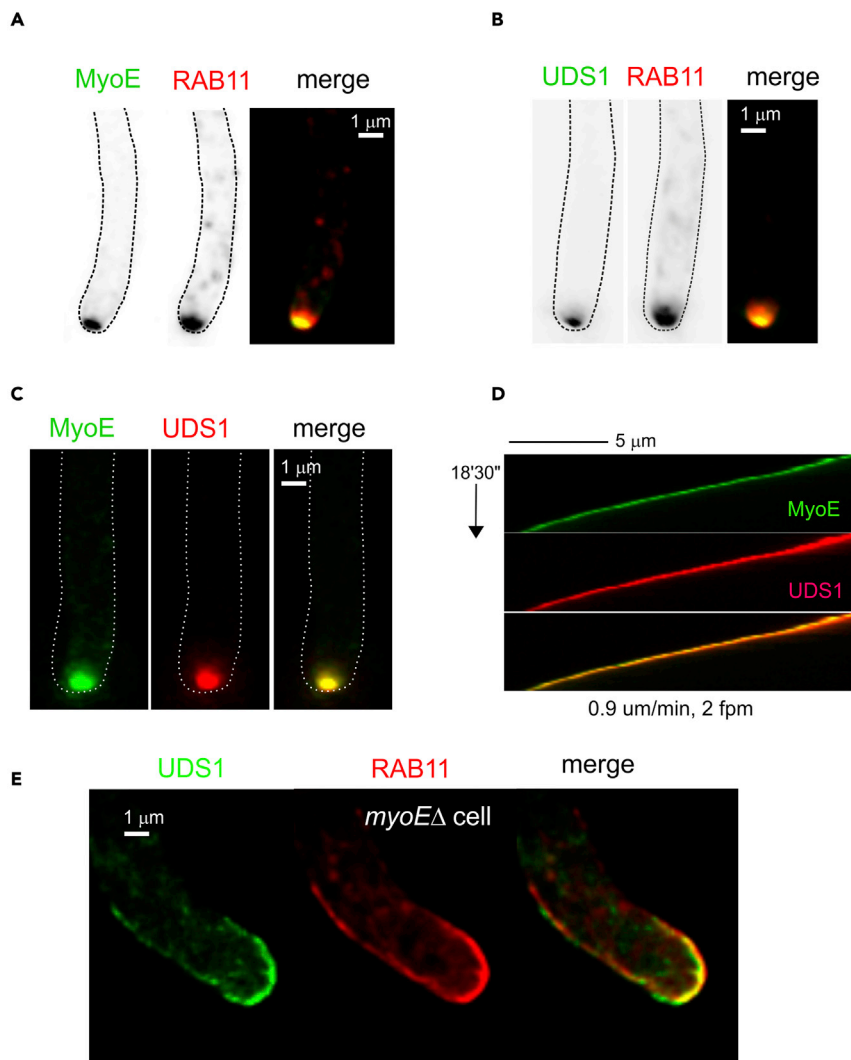


Figure 3. Subcellular localization of UDS1

(A) Hyphal tip cell expressing mCh-RAB11 and MyoE-GFP; images are MIPs of deconvolved Z-stacks, all at the same magnification.

(B) A hyphal tip cell expressing mCh-RAB11 and UDS1-GFP. Images are MIPs of deconvolved Z-stacks. See also [Video S5](#).

(C) Left, a hyphal tip cell expressing endogenously tagged MyoE-GFP and UDS1-tdT. Images are MIPs of deconvolved Z-stacks.

(D) MyoE-GFP and UDS1-tdT strictly colocalize across time: A 4D movie made with MIPs of Z-stacks acquired every 30 s ([Video S6](#)) was used to draw a kymograph across the long axis of a hypha growing at 0.9 μm/min. The diagonal lines traced by apical spots reflect apical extension growth.

(E) UDS1-GFP strictly colocalizes with mCh-RAB11 SVs transported by MTs to the apical dome in a cell lacking MyoE. Images are MIPs of deconvolved Z-stacks. See also [Video S7](#).

AlphaFold to predict the 3D organization, and secondary structure elements of HMSV ([Figure 4C](#); [Figures S3C](#) and [S3D](#)) display the confidence tests for the prediction. AlphaFold identifies eight potential α -helices, of which helices V, VII, and VIII (the latest containing the C-terminus) form a three-helical coiled-coil. The long helix II ([Figure 4C](#)) appears free to establish protein-protein interactions. As anticipated by COIL, the protein also contains two long disordered regions, one corresponding to the N-terminal 350-residue region and a second to residues 551–625 ([Figure 4C](#)). Proteins containing disordered regions associate spontaneously. These intrinsically disordered proteins are associated with a score of processes and are thought to promote liquid-liquid phase separation that could be the basis for the organization of membrane-less organelles ([Musacchio, 2022](#)). These observations were appealing, as HMSV, like UDS1,

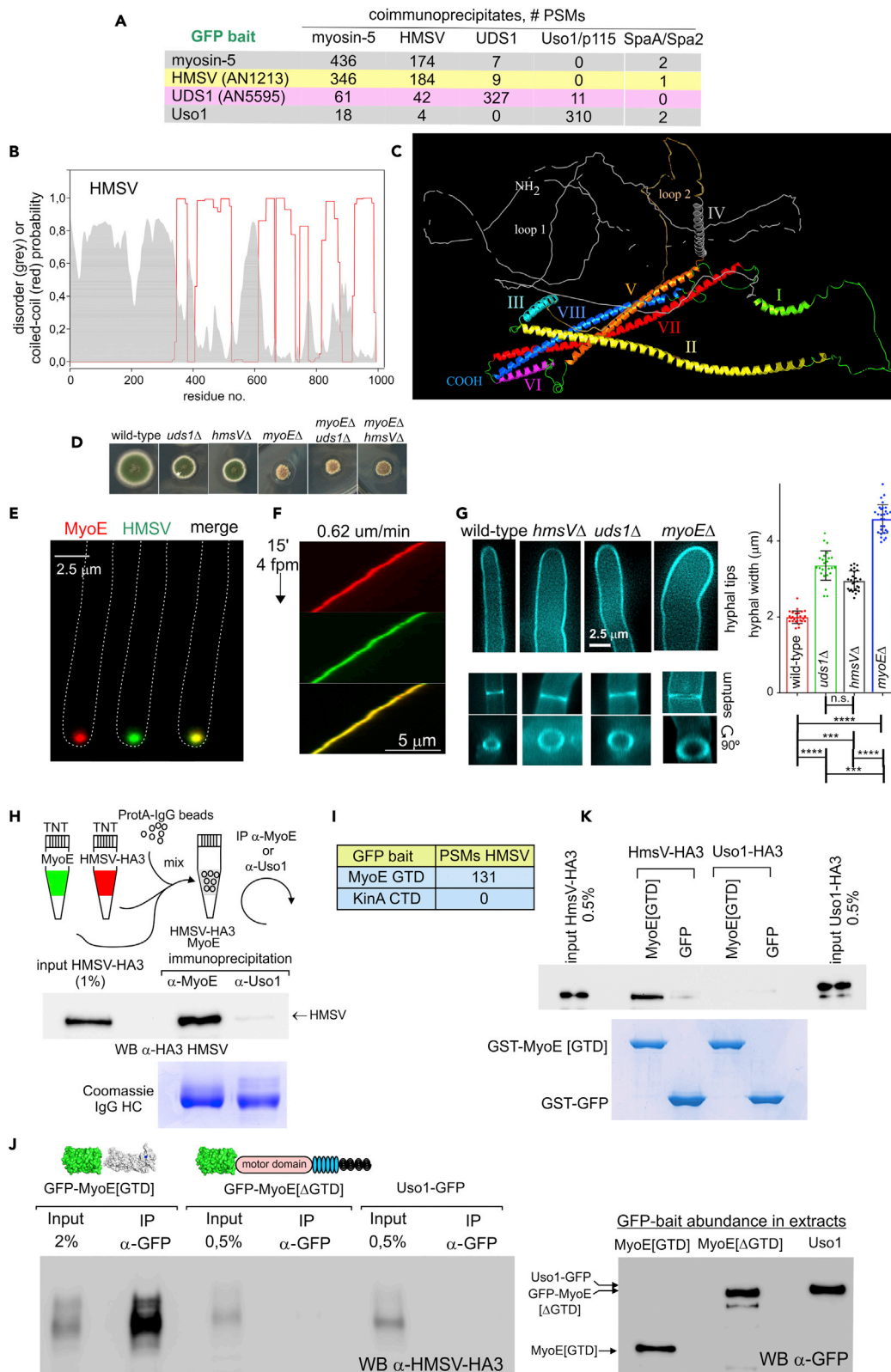


Figure 4. HMSV, an uncharacterized interactor of the MyoE GTD

- (A) Cell extracts expressing the indicated GFP-tagged baits by allelic replacement were immunoprecipitated with GFP-Trap. Pulled-down proteins were analyzed by LC-MS/MS. The table lists the spectral counts obtained for each of the indicated co-precipitating proteins. A *Uso1*-GFP-expressing strain was used as negative control.
- (B) Prediction of coiled-coils (red graph) and disordered regions (gray area) along the primary sequence of HMSV.
- (C) AlphaFold prediction of HMSV. Roman numerals indicate α -helical regions (color-coded). Two large disordered regions are indicated as loop 1 and loop 2. See also [Figures S3C and S3D](#).
- (D) Growth tests at 37°C of indicated strains. See also [Figure S1B](#).
- (E) Endogenously tagged MyoE-mCh and HMSV-GFP strictly colocalize. MIPs of deconvolved Z-stacks.
- (F) Kymograph derived from the 4D sequence shown in [Video S8](#), mounted with MIPs of Z-stacks acquired with a beam splitter every 15 s for 15 min. The hypha was growing at 0.62 $\mu\text{m}/\text{min}$.
- (G) Widths of wild-type and mutant hyphae stained with calcofluor to label the cell walls. Top, middle planes of representative tips. (Bottom) x,y images of septa alongside with the corresponding orthogonal views. (Right) Quantitation of cell width. Bars are the average value for ~ 20 hyphae per condition; error bars are SD. Significance was assessed with an ANOVA Kruskal-Wallis test with Dunn's multiple comparison correction. n.s., not significant.
- (H) MyoE and HMSV interact directly: MyoE and HMSV-HA3 obtained from TNT reactions were mixed with Protein A beads preloaded with polyclonal α -MyoE antiserum or with antiserum against the unrelated protein *Uso1*. Immunoprecipitates were analyzed by α -HA western blotting. Equal IgG loading was confirmed with Coomassie-stained heavy chains.
- (I) Spectral counts of HMSV detected in GFP-trap immunoprecipitates of cell extracts expressing the MyoE GTD or the analogue cargo-binding, C-terminal domain (CTD) of *KinA/kinesin-1*.
- (J) HMSV associates with MyoE through the GTD of the motor. Extracts of *myoE Δ* cells co-expressing HMSV-HA3 with GFP-tagged MyoE GTD or MyoE Δ GTD (MyoE lacking the GTD) were immunoprecipitated with GFP-Trap nanobody. A *Uso1*-GFP HMSV-HA3 strain was used as negative control. (Left) Pulled-down material was analyzed by α -HA western blotting. (Right) Relative levels of the preys by α -GFP western blotting.
- (K) HMSV interacts directly with the MyoE GTD: pull-down assays with indicated GST baits. Preys were *in vitro* expressed (with TNT) HMSV-HA3 or, as control, *UDS1*-HA3. Blots were revealed with α -HA antibody.

localizes to the SPK, strictly colocalizing with MyoE during hyphal growth ([Figures 4E, 4F and Video S8](#)). To determine the consequences of removing *UDS1* and HMSV, we constructed strains carrying null *uds1 Δ* and *hmsV Δ* alleles. These are phenotypically indistinguishable, resulting in a radial colony growth defect ([Figure 4D](#)), and, at the cellular level, in abnormally wide hyphae ([Figure 4G](#)), both features indicative of defective exocytosis. Notably, the colony growth defect resulting from *uds1 Δ* and *hmsV Δ* was markedly weaker than that caused by *myoE Δ* . Double *uds1 Δ* *hmsV Δ* mutants behaved like the parental single mutants, consistent with the corresponding products being components of the same functional unit ([Figure S1B](#)). The fact that both *uds1 Δ* and *hmsV Δ* are hypostatic to *myoE Δ* ([Figure 4D](#)) suggested that this hypothetical complex acts through MyoE, although neither *UDS1* nor HMSV plays an essential role in MyoE function.

The high yields of HMSV and MyoE recovered with their respective GFP-trap immunoprecipitates suggested that MyoE and HMSV are direct interactors ([Figure 4A](#)). This prediction was confirmed by co-immunoprecipitation experiments using MyoE and HMSV-HA3 expressed by coupled transcription-translation reactions primed with their respective cDNAs. The two proteins were combined and immunoprecipitated with α -MyoE-specific IgGs or with IgGs raised against the unrelated protein *Uso1* (acting in the ER/Golgi interface). α -MyoE IgGs, but not α -*Uso1* IgGs, immunoprecipitated HMSV-HA3 ([Figure 4H](#)), establishing that HMSV and MyoE interact directly. GFP-trap co-immunoprecipitation coupled to MS/MS showed that the GFP-MyoE [GTD] construct discussed in [Figure 1](#), but not a similar construct carrying the carboxy-terminal region of *KinA* (*kinesin-1*), efficiently pulled down HMSV, strongly indicating that MyoE uses its GTD domain to interact with HMSV ([Figure 4I](#)). Next, we determined, using GFP-TRAP immunoprecipitation experiments of cell extracts (of *myoE Δ* cells, to avoid heterodimerization) expressing either the GFP-MyoE [GTD] construct or the complementary GFP-tagged MyoE [Δ GTD] construct (*i.e.* the motor, IQ repeats and coiled-coil domains, without the GTD), that the GTD domain of MyoE is necessary and sufficient to interact with HMSV ([Figure 4J](#)). That this interaction is direct was further established after reconstructing the interaction *in vitro* using purified GST-GTD and *in vitro* synthesized HMSV. GST-GTD beads pulled down HMSV but not the unrelated prey *Uso1*, whereas neither prey was pulled down by GST-GFP, demonstrating specificity ([Figure 4K](#)). Thus, HMSV interacts directly with the GTD of MyoE, which together with data above suggested that HMSV acts as a connector between *UDS1* and MyoE (to be reinforced below).

The MyoE-containing complex HUM is a RAB11 effector scaffolded by HMSV

Unlike *UDS1*, HMSV did not appear to interact with RAB11 in shotgun proteomic experiments ([Figure 2A](#)). To confirm this observation, we performed more sensitive GST-pull down assays with whole cell extracts expressing HA3-tagged preys. Under conditions in which *UDS1*-HA3 strongly associated with RAB11-GST, HMSV-HA3 did not ([Figures 5A and 5B](#)). We noted, however, that strong overexposure of the blots

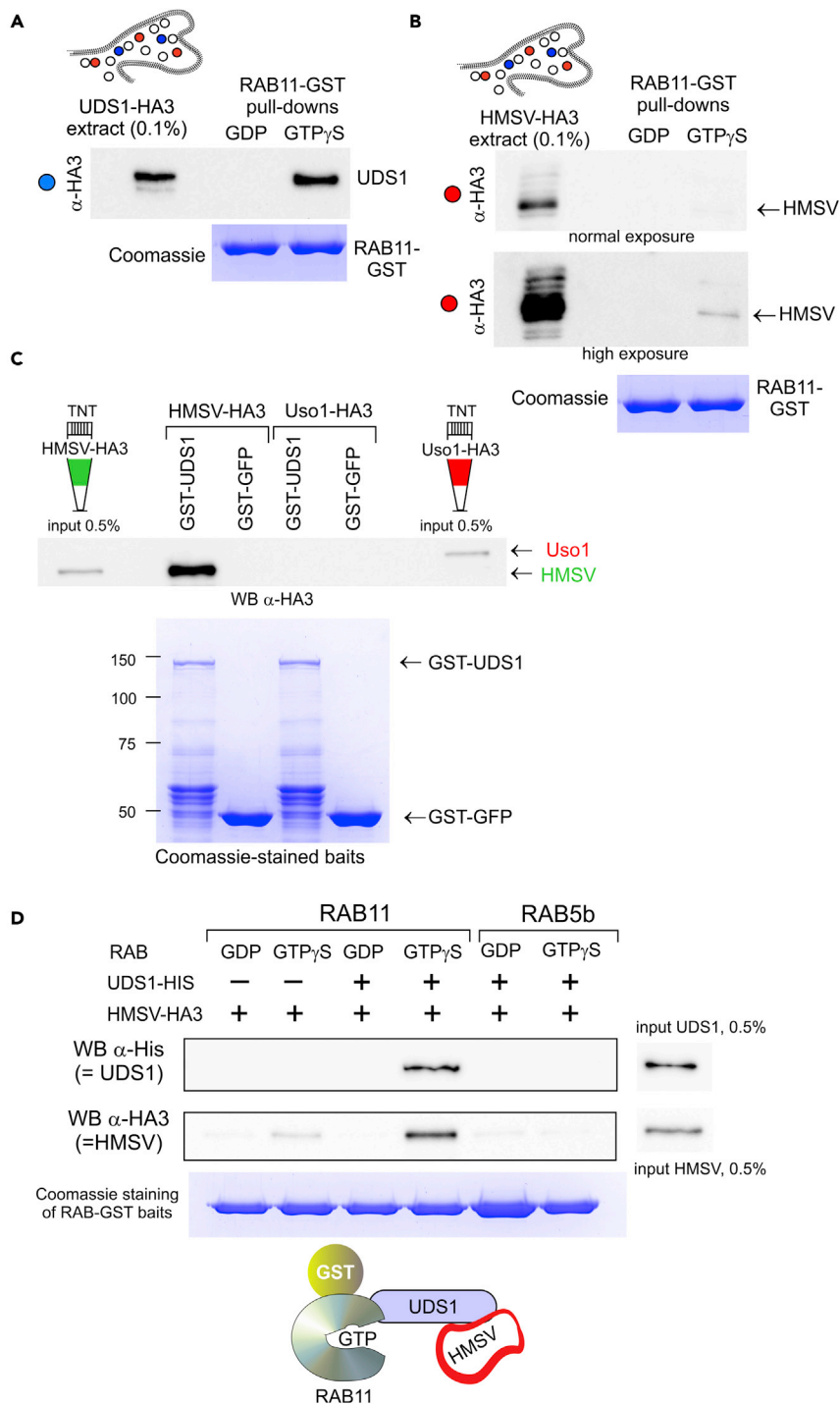


Figure 5. UDS1 bridges its direct interactor HMSV to the active form of RAB11. HMSV does not interact directly with RAB11

(A) Control showing that a Uds1-HA3 is efficiently pulled down from extracts by GTP γ S RAB11 but not by GDP-RAB11. (B) As in (A), but using HMSV-HA3 extracts as preys. Uds1-HA3 and HMSV-HA3 were expressed from allelic replacements. Pull-downs analyzed by α -HA western blotting.

(C) HMSV and UDS1 interact directly: pull-down assays with GST-UDS1 as bait and HMSV-HA3 or, as negative control, Uso1-HA3 as preys, which were obtained by TNT expression. Pull-downs analyzed by α -HA3 western blotting.

Figure 5. Continued

(D) HMSV is recruited to RAB11 only when UDS1 is present and the GTPase is in the active conformation. GST pull-down assays with RAB11 and, as negative control, RAB5b baits. The preys, combined as indicated, were purified UDS1-His and TNT-synthesized HMSV-HA3. Samples were analyzed by α -His and α -HA western blotting.

revealed a very faint signal in the GTP γ S-RAB11 lane, arguing against HMSV being a direct interactor of RAB11 and suggesting instead that another factor(s)/component(s) of the HMSV-MyoE complex present in the reaction mixtures (note that total cell extracts—not purified proteins—were used as preys in this experiment) might bridge HMSV to RAB11, albeit inefficiently (see discussion). While an indirect linker of HMSV to RAB11 was MyoE, shotgun proteomic experiments with GFP traps (Figure 4A) suggested that UDS1 contributes to this bridging role. Figure 5C shows that GST-UDS1, but not the unrelated bait GST-GFP, pulled-down *in vitro* synthesized HMSV-HA3. In contrast, neither bait pulled-down Uso1-HA3, confirming specificity and establishing that UDS1 and HMSV interact directly. Therefore, through its capacity to bind directly to both MyoE and UDS1, HMSV would act as scaffold of a heteromeric complex that would be recruited by RAB11 to SVs by contacting both UDS1 and MyoE.

This model was tested with two sets of experiments. First, we demonstrated *in vitro* that HMSV is recruited to active RAB11 only if UDS1 is present to bridge the interaction (Figure 5D). To this end, we performed GST-RAB pull-downs in the presence of bacterially expressed UDS1, *in vitro* synthesized HMSV-HA3 or both. HMSV was recruited by GTP γ S-RAB11, but did so only when UDS1 was present in the reaction mix. Neither conformation of RAB5b nor GDP-RAB11 pulled-down HMSV even when UDS1 was present. We conclude that the presence of UDS1 is sufficient for the efficient recruitment of HMSV by the active form of RAB11, establishing that HMSV is an indirect effector of the latter.

Secondly, we demonstrated that a stable complex consisting of MyoE, HMSV and UDS1 is present in cellular lysates, and that this complex, that we denoted HUM (for HMSV-UDS1-MyoE) is scaffolded by HMSV. As determined by anti-MyoE Western blotting of GFP-Trap immunoprecipitates of whole-cell extracts, MyoE strongly associates with UDS1-GFP and with HMSV-GFP, but not with the unrelated bait Uso1-GFP (Figure 6A). Indeed, MyoE association with UDS1 and HMSV is so efficient that co-immunoprecipitated MyoE could be visualized directly by silver-staining of SDS-PAGE gels (Figure 6A, right). Despite HMSV appearing to be the less abundant of the three baits (anti-GFP western blot, Figure 6A, right), HMSV pulled down MyoE markedly more efficiently than UDS1 did, in agreement with the conclusion that MyoE and UDS1 interact indirectly by way of HMSV. Consistently, the interaction between MyoE and UDS1 was undetectable with *hmsV* Δ extracts (i.e. was completely dependent on the presence of HMSV) (Figure 6B), whereas that between MyoE and HMSV was completely independent of UDS1, taking place irrespectively of whether wild-type or *uds1* Δ extracts were used (Figure 6C). Lastly, the interaction between UDS1-GFP and HMSV-HA3 was completely independent of MyoE (Figure 6D), as predicted by *in vitro* reconstitution experiments above.

Taken together these data show that these proteins form a complex in the order MyoE/HMSV/UDS1 that has the dual ability to interact with the active form of RAB11 through UDS1- and MyoE-mediated contacts.

Evidence that UDS1 and HMSV assist RAB11 to recruit MyoE to SVs

A diagnostic readout of MyoE transport is the focusing of SVs at the SPK. Consistent with UDS1 and HMSV acting in a complex regulating myosin V transport, both *uds1* Δ and *hmsV* Δ affected RAB11 SVs similarly, reallocating them from the SPK to a crescent-shaped distribution in the apical dome typical of impaired MyoE function (Figure 7A). This effect was markedly less conspicuous than that caused by *myoE* Δ , which resulted in a broader crescent and, as discussed above, in a marked reduction of the signal of SVs docked at the tip cortex (Figure 1B). Therefore, these data strongly indicate that myosin V transport is debilitated in *uds1* Δ and *hmsV* Δ mutants, such that although this transport is not abolished, MT-mediated transport gains prominence, which results in targeting SVs to a broad surface determined by the sites at which MTs' plus ends reach the apical dome. Impairment of actomyosin transport in these mutants explains the partial exocytic deficit that growth tests and hyphal morphologies indicate (Figures 4D and 4G).

The above experiments suggested that the UDS1 and HMSV subunits of HUM might play the role of a co-receptor reinforcing the RAB11-mediated recruitment of MyoE to SVs. Myosin V dwells in an inactive conformation that is shifted to the active conformation by cargo (Donovan and Bretscher, 2015a). Thus, a deficit in cargo loading would be translated into a drop in MyoE activity, which should in turn result in

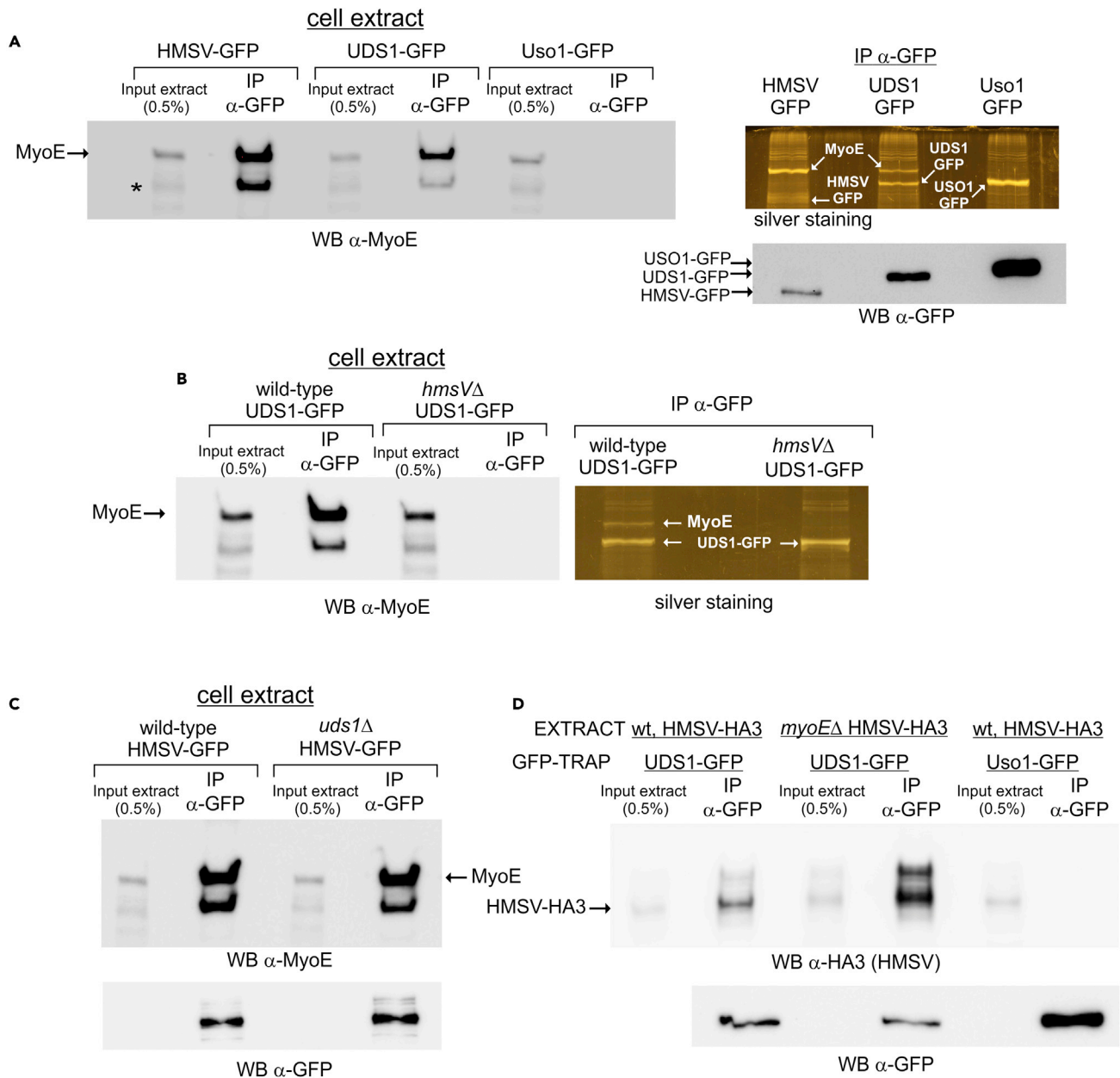


Figure 6. UDS1 and MyoE are components of the HMSV-scaffolded HUM complex

(A) MyoE associates with UDS1 and HMSV. Extracts of cells expressing endogenously tagged GFP proteins were immunoprecipitated with α -GFP nanobody. (Left) α -MyoE western blot analysis of immunoprecipitates. The band indicated with an asterisk is unspecific (α -MyoE is a polyclonal antiserum). (Right top) Silver staining of immunoprecipitates. MyoE is remarkably abundant in the HMSV sample, detectable in the UDS1 sample, and absent in the Uso1 sample. (Right bottom) Relative levels of the preys revealed by α -GFP western blotting.

(B) UDS1 and MyoE associate only if HMSV is present.

(C) HMSV and MyoE associate efficiently when UDS1 is absent.

(D) UDS1 associates with HMSV regardless of whether MyoE is absent or present. GFP-Trap immunoprecipitates were analyzed by α -HA3 western blotting to detect HMSV and by α -GFP western blotting to reveal the relative levels of the baits.

a reduction in the levels of MyoE at the SPK. [Figure 7A](#) shows that both *uds1Δ* and *hmsVΔ* reduce the SPK MyoE signal by 5- to 6-fold, supporting the contention that in these mutant backgrounds the engagement of SVs with MyoE is compromised. [Video S9](#) comparing the wild-type with an *hmsVΔ* strain depicts the impaired delivery of MyoE to the SPK in the mutant. MyoE SVs are visible in these movies.

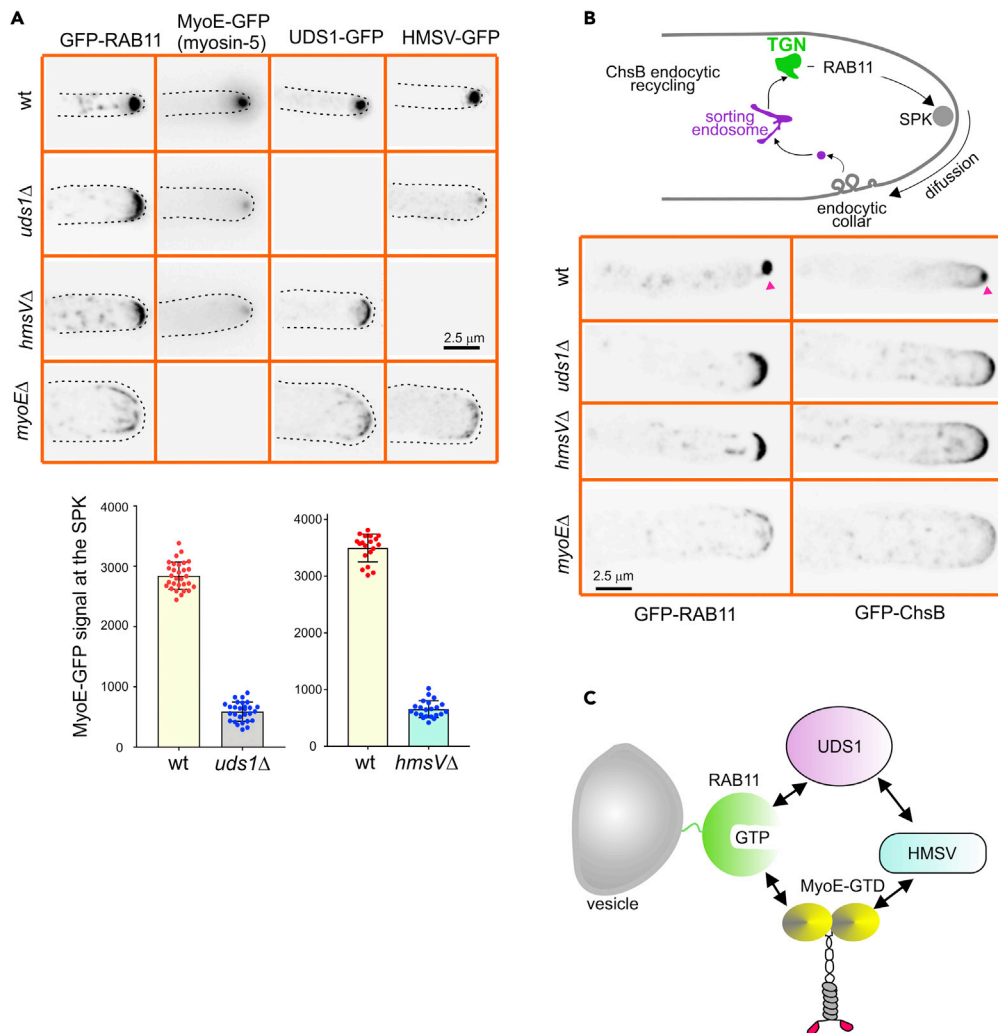


Figure 7. HUM complex components cooperate with RAB11 to recruit MyoE to SVs. A model

(A) (Top) Localization of the HUM complex components in different genetic backgrounds. Images are MIPs of deconvolved Z-stacks. As GFP reporters were endogenously tagged, the corresponding null background images are empty. (Bottom) Quantitation (arbitrary units, A.U.) of the MyoE-GFP signal in the SPK of *uds1Δ* and *hmsVΔ* cells compared with the wild type. Means (\pm SD) were: left, wild-type $2,842 \pm 227$ versus *uds1Δ* 558 ± 159 ($p < 0.0001$ in unpaired t test). (Right) Wild type, $3,496 \pm 245$ versus 654 ± 149 in the *hmsVΔ* mutant ($p < 0.0001$ in unpaired t test). See also Videos S9 and S10.

(B) A prototypic cargo of the RAB11 recycling pathway is delocalized from the SPK by *uds1Δ* and *hmsVΔ*. The scheme depicts endocytic recycling followed by the chitin-synthase ChsB. ChsB and RAB11 are similarly delocalized from the SPK, indicated by red arrowheads.

(C) Model for the engagement of HUM with RAB11 SVs. In the wild type, RAB11 is recruited to SVs during the Golgi-to-post-Golgi transition. RAB11 interacts both with the GTD of MyoE and with UDS1 in the HUM complex. UDS1 bridges active RAB11 to the HMSV scaffold. HMSV bridges RAB11/UDS1 to MyoE by direct interaction with the motor's GTD. MyoE transport is most efficient in the context of the whole complex. However, in the absence of UDS1 or HMSV, MyoE-mediated SV transport remains partially operative due to the direct interaction between RAB11 and the MyoE GTD, albeit this transport is less efficient, accumulation of SVs in the SPK is impaired and MT-dependent transport becomes more prominent, leading to the characteristic apical dome distribution of SVs in these mutants.

We next investigated the dependence of UDS1 and HMSV on each other. In *hmsVΔ* cells UDS1 delocalized from the SPK to an apical crescent remarkably similar to that observed with RAB11 in *hmsVΔ* and *myoEΔ* backgrounds (Figures 7A and 3E). The finding that UDS1 ‘goes with’ RAB11 is consistent with the prediction that the connection of UDS1/RAB11 SVs with MyoE should be impaired by *hmsVΔ* (a broader distribution indicates that the balance between actomyosin and MT transport has been shifted toward the latter). In

sheer contrast, HMSV is not delocalized from the SPK in *uds1Δ* cells, but the signal was reduced to an extent roughly commensurate with the reduction in MyoE signal (Figure 7A), indicating that HMSV goes with the proportion of MyoE that is (less efficiently) loaded with cargo by way of the direct interaction of RAB11 with the motor, and therefore that HMSV binds to RAB11 by way of UDS1. Notably, the localization of HMSV in *myoEΔ* cells is remarkably similar to that of RAB11 and UDS1 (Figure 7A) (Video S10 for HMSV). Thus, without MyoE the other HUM complex components associate with RAB11 and are delivered to the PM by MT transport, which results in their localization to the apical dome. This observation further demonstrates that UDS1 and HMSV are components of RAB11 SVs rather than structural constituents of the SPK.

Ablation of UDS1 or HMSV impairs the delivery of an exocytic cargo to the SPK

A well characterized cargo of RAB11 SVs is the chitin synthase ChsB (Hernández-González et al., 2018a). This integral membrane protein is exocytosed to the apical PM by way of the SPK, diffuses away from the tip and it is taken up by a highly active endocytic collar that transports it to a sorting endosome. From this compartment ChsB returns to the TGN where it is incorporated into RAB11 SVs delivered to the SPK (Figure 7B). In the wild-type, a proportion of ChsB is present in the SPK. In *uds1Δ* and *hmsvΔ* cells this accumulation of ChsB in the SPK is no longer seen, resembling the situation with RAB11, which is included in Figure 7B for comparison. We interpret that the absence of the UDS1/HMSV co-receptor role affects transport of a RAB11 cargo from the TGN to the SPK.

In summary, our data strongly support a model in which HMSV and UDS1 are components of a MyoE-containing complex that we denoted HUM and that is recruited by RAB11 to SVs through direct interactions with both UDS1 and MyoE. HMSV/UDS1 serves as a co-adaptor between these vesicles and the motor (Figure 7C). When this co-adaptor is disorganized by ablation of either of its two components, actomyosin transport of these SVs still occurs, albeit less efficiently, due to the direct interaction between RAB11 and MyoE.

DISCUSSION

The ability of type V myosins to transport cargo is crucial for the biogenesis and distribution of membranous compartments (Hammer and Sellers, 2012; Wong and Weisman, 2021). *A. nidulans* has a single type V myosin, MyoE (Taheri-Talesh et al., 2012), implying that specificity for different cargoes must be mediated by different adaptors (Cross and Dodding, 2019; Wong and Weisman, 2021). Adaptors often involve a RAB family member, as individual RABs display a high selectivity for their cognate membrane compartment (Pfeffer, 2013; Pinar and Peñalva, 2021). RABs can interact directly with myosin V or, indirectly, by means of intermediate proteins that bridge the activated RAB and the motor (Hammer and Sellers, 2012; Wong and Weisman, 2021). A well understood co-adaptor is melanophilin bridging RAB27 on melanosomes to MyoVa (Wu et al., 2002).

Even if the binding of the RAB to the type V myosin is direct, it might involve co-adaptors that help stabilizing the complex. This is the case of metazoan RAB11, FIP2 and MyoVb (FIP2 is a direct effector of RAB11), which form a tripartite complex required for traffic between recycling endosomes and the PM (Hales et al., 2002; Li et al., 2007; Schafer et al., 2014; Wang et al., 2008). In addition to complex stabilization, co-adaptors play additional roles. The C-terminal region of melanophilin binds F-actin, dramatically increasing the processivity of MyoVa (Sckolnick et al., 2013). Moreover, melanophilin tracks, by hitchhiking on EB1, the plus-ends of MTs, recruiting MyoVa to them, which might ensure the efficient transfer of melanosomes from MTs to actin cables (Wu et al., 2005). Another example of additional functions of RAB-containing type V myosin adaptors occurs in mouse oocytes, where MyoVa is recruited to RAB11 vesicles by cooperative interactions with both the GTPase and the actin nucleator SPIR-2, which help to coordinate MyoVa vesicle transport with actin nucleation (Pylypenko et al., 2016). Adaptors may also play roles unrelated to transport. For example, phosphorylation and ubiquitin-mediated degradation of the yeast vacuolar adaptor Vps17 is required to release the organelle from Myo2 (Wong et al., 2020).

In *A. nidulans*, the biogenesis of SVs dispatched to the PM by way of the SPK (a vesicle supply center located underneath the apical plasma membrane) is mediated by RAB11. These SVs are loaded with the type V myosin MyoE, kinesin-1 (KinA) and dynein (Pantazopoulou et al., 2014; Peñalva et al., 2017), yet the adaptors linking these molecular motors to SVs remain uncharacterized. One current model proposes that, resembling melanosome transport, kinesin-1 hauls SVs to tip-proximal regions before transferring them to MyoE, which concentrates them at the SPK (arguably the analogue of the cell periphery in melanosomes) (Pantazopoulou et al., 2014). This two-step mechanism would involve the transfer of SVs from

MT-to F-actin-mediated transport, a relay that would be compromised by the high density of cytoskeletal tracks and organelles populating the hyphal tip. This model accounts for the synthetic lethal phenotype displayed by *kinAΔ myoEΔ* double mutants (Peñalva et al., 2017; Zhang et al., 2011) and is supported by the finding that SVs are loaded with both MT-dependent (kinesin-1, dynein) and F-actin-dependent motors (myosin V) (Pantazopoulou et al., 2014), which would enable them to switch from MTs to F-actin directly. However, an alternative model would account for the lethality resulting from *kinAΔ myoEΔ*, namely that myosin V transport acts in parallel to kinesin-1, such that instead of receiving SVs from the latter, myosin V would be able to attach and transport them directly to the tip, at least from the apicalmost proximal TGN cisternae. This second model is supported by the observation that the area occupied by RAB11 at the tips extends beyond that occupied by MyoE, which is restricted to the SPK. Thus, at least some MT-dependent transport reaches the PM directly by MTs, without involving actomyosin transport.

Here we characterized HUM, a heteromeric complex minimally containing MyoE and two coiled-coil proteins, HMSV and UDS1, but almost certainly including other factors such as calmodulin and myosin light chains. HUM is recruited to SVs through direct interactions between both MyoE and UDS1 and the active GTP conformer of RAB11, the GTPase governing traffic between the TGN and the SPK (Pantazopoulou et al., 2014; Peñalva et al., 2017; Pinar et al., 2015). RAB11 interacts both with the GTD domain of MyoE and with UDS1, the MyoE GTD interacts both with RAB11 and with HMSV, and HMSV scaffolds the complex by interacting with both UDS1 and the MyoE GTD, but not with RAB11 [RAB11 cannot possibly interact with more than two effectors simultaneously, see (Burke et al., 2014; Vetter et al., 2015)]. The MyoE GTD domain binding RAB11 is also necessary and sufficient to recruit HMSV, emphasizing the role of this domain as an interaction hub. Amino acid sequences of the mammalian MyoVa,b,c and fungal Myo2 and MyoE GTDs are conserved (Pashkova et al., 2006; Pylypenko et al., 2013).

In *hmsVΔ* cells, UDS1-GFP distributes like RAB11 whereas in *uds1Δ* cells HMSV-GFP distributes like myosin V, suggesting that the HUM complex can be split in two stable subcomplexes, nucleated by RAB11-GTP and by MyoE-GTD, respectively. Therefore, both UDS1 and HMSV are necessary for the assembly of a HUM, whose absence debilitates F-actin-mediated transport, as reflected in the spreading of RAB11 SVs across the apical dome. Inefficient F-actin transport of RAB11 resulting from ablation of UDS1 or HMSV correlates with slower colony growth, and spreading of RAB11 SVs across the hyphal tip dome correlates with delocalization of its cargo, ChsB, from the SPK. Of note, myosin V transport is not abolished in the absence of HUM, possibly because RAB11 is able to bind MyoE directly, which makes the phenotypic consequences of ablating UDS1 or HMSV less severe than those resulting from removing MyoE. That MyoE recruitment by Sec4 does not appear to involve HUM (Figure 2H) in all likelihood also contributes to the relatively weak growth phenotypes of *uds1Δ* and *hmsVΔ*.

Cargo adaptors for myosin V are difficult to identify by primary sequence- or domain composition-based searches (Wong and Weisman, 2021). Both UDS1 and HMSV are coiled-coil proteins, which frequently serve as adaptors of molecular motors, including myosin V (Cross and Dodding, 2019). A well-understood example is the coiled-coil melanosome protein RILPL2 (RAB interacting lysosomal protein-like 2) bridging RAB36 with the MyoVa GTD (Matsui et al., 2012; Wei et al., 2013).

While our data clearly implicate the HUM complex in adapting MyoE to RAB11 SVs, we cannot rule out that, in addition, UDS1 and HMSV play non-receptor roles, such as retaining SVs in the SPK, either directly or through its regulation of F-actin microfilaments at the core of the SPK. This F-actin regulatory role would be supported by the presence of the polarisome component Spa2 as an associate of the *N. crassa* MYO-5/JANUS-1/SPZ-1 complex (Zheng et al., 2020). However, *A. nidulans* SpaA (=Spa2) does not copurify with MyoE/UDS1/HMSV, and SepA, the only formin of *Aspergillus*, localizes to the SPK in a SpaA-independent manner (Virag and Harris, 2006). These two facts, together with the absence of a Pea2 equivalent in *Aspergillus*, strongly argue against equivalent roles of the polarisome in *A. nidulans* and *S. cerevisiae*. Of note, Zheng et al. (2020) concluded that MYO-5/JANUS-1/SPZ-1 is not involved in vesicle trafficking, unlike the *Aspergillus* HUM complex.

An appealing yet highly speculative possibility is that RAB11 co-adaptors contribute to the organization of the SPK by promoting liquid-liquid phase partition to form a membraneless organelle. Alpha-Fold prediction indicates that HMSV is composed of coiled-coils and long unstructured regions, of which the most conspicuous corresponds to the N-terminal 350 amino acids. Intrinsically disordered proteins are frequent dwellers of membraneless compartments supposedly mediating liquid-liquid demixing that results in phase separation (Musacchio, 2022).

UDS1 and/or HMSV might also contribute to the efficiency of myosin V transport. In the absence of MyoE, RAB11 SVs decorate the array of tip actin cables radiating from the SPK (Pantazopoulou et al., 2014), suggesting that these vesicles contain an F-actin-binder. It is tempting to speculate that UDS1 or HMSV resemble melanophilin (Sckolnick et al., 2013) or the Sec4p-Myo2p accessory factor Smy1p (Hodges et al., 2009; Lwin et al., 2016) in that they interact with actin cables to increase the processivity of the motor. Alpha-Fold prediction of UDS1 buttressed by analytical ultracentrifugation and EM studies strongly suggested that this protein is an elongated (circa 500 Å-long) dimer formed by a long coiled-coil core. Each UDS1 domain is formed by three small helices associating with those of the second domain to form a V-shaped 'wing' that protrudes from the long axis. We speculate that this long structure could play a tethering role, for example by providing an ATPase cycle-independent hold of the motor to F-actin filaments. Even more suggestive is the hypothetical possibility that F-actin binding by the MyoE co-adaptors facilitates the switch between MT and F-actin transport. It should be noted that Sec4 cannot recruit UDS1, which is consistent with the view that *A. nidulans* Sec4 acts downstream of the RAB11-mediated transport of SVs to the SPK, mediating the ultimate step of exocytosis (Pinar and Peñalva, 2021).

In summary, we have identified HUM, a novel myosin-V-containing complex required for the efficient coupling of RAB11 SVs to MyoE. Proof of concept that a motor-cargo interface can be targeted by a small chemical has been recently provided (Randall et al., 2017). Although speculative, the possibility of interfering with fungal growth by diminishing the efficiency of myosin-V-mediated transport is appealing.

Limitations of the study

Structures of the RAB11 accessory factors should inspire experiments addressing their mechanistic roles. Our approaches to the UDS1 structure including size exclusion chromatography, analytical ultracentrifugation, and negative-staining EM of the purified protein strongly supports the AlphaFold model. However, the intrinsic flexibility of UDS1 precluded any attempt to average molecule shapes. Moreover, the 3D structure of HMSV relies solely on AlphaFold, because the protein is insoluble when expressed in bacteria. Our inability to obtain HMSV in quantities required for its structural characterization and for reconstituting the whole transport process by bottom-up synthetic approaches is currently a bottleneck. Secondly, as already mentioned, the HUM complex in all likelihood has other partners that cannot be reliably identified by GFP-trapping and MS/MS, perhaps due to the very transient interactions in which they are engaged. A third caveat is that our current data do not discriminate between a "relay model" for the cooperation between actin and MTs and a "parallel pathways model" in which myosin V would deliver SVs to the vesicle supply center (SPK), whereas kinesin-1 would deliver SVs directly to the cell cortex at the sites of MT plus-end contacts (A hybrid model is also possible).

STAR★METHODS

Detailed methods are provided in the online version of this paper and include the following:

- KEY RESOURCES TABLE
- RESOURCE AVAILABILITY
 - Lead contact
 - Materials availability
 - Data and code availability
- EXPERIMENTAL MODEL AND SUBJECT DETAILS
 - Aspergillus techniques
 - Null mutant strains and protein tagging
- METHOD DETAILS
 - GFP-MyoE GTD and GFP-MyoE ΔGTD transgenes driven by the *inuA* promoter
 - Plasmids for protein expression
 - *In vitro* transcription/translation
 - Antibodies and western blotting
 - Western blots were reacted with the following antibodies
 - RAB-GST purification and nucleotide loading
 - UDS1-His6 expression and purification from bacteria
 - RAB-His6 purification and nucleotide loading
 - Total cell extracts
 - RAB-GST pull-downs with total cell extracts

- RAB-GST pull-downs with purified proteins
- Pull-down of the UDS1-HMSV complex with RAB11-GST
- Pull-down experiments of TNT-expressed proteins with GST fusion protein baits
- Pull-down experiments of RAB preys with GST-GTD
- ProtA immunoprecipitations
- GFP-trap and western blotting
- Shotgun proteomic analysis of RAB11-GST effectors
- Analytical ultracentrifugation
- Negative staining electron microscopy
- Fluorescence microscopy
- Alpha-Fold predictions
- **QUANTIFICATION AND STATISTICAL ANALYSIS**

SUPPLEMENTAL INFORMATION

Supplemental information can be found online at <https://doi.org/10.1016/j.isci.2022.104514>.

ACKNOWLEDGMENTS

We thank Juan M. Luque (Molecular Interactions Facility, Centro de Investigaciones Biológicas) for his help with equilibrium sedimentation analyses, Elena Reoyo for skillful technical assistance, and Herb Arst for critical reading of the manuscript. Thanks are due to Spain's Ministerio de Ciencia e Innovación for grants RTI2018-093344-B100 (MAP) and BFU2017-89143-P (EA-P), as well as for grant-associated Predoctoral contracts BES-2016-077440 (IB.-P/MAP) and PRE2018-086026 (to AG/EA-P). Thanks are also due to the Comunidad de Madrid grant for S2017/BMD-3691 (MAP). Grants were co-funded by European Regional Development and European Social Funds. The authors declare that they do not have any competing financial interests.

AUTHOR CONTRIBUTIONS

MP, AA, and IB-P carried out biochemical and genetic experiments. VdR conducted MS/MS analyses; EA-P and AdG conducted electron microscopy experiments, AG conducted AlphaFold predictions, and MAP carried out fluorescence protein localization analyses, supervised the project, and, with MP, wrote the manuscript with input from all authors.

DECLARATION OF INTERESTS

The authors declare no competing interests.

Received: March 1, 2022

Revised: March 28, 2022

Accepted: May 26, 2022

Published: July 15, 2022

REFERENCES

- Abenza, J.F., Galindo, A., Pantazopoulou, A., Gil, C., de los Ríos, V., and Peñalva, M.A. (2010). *Aspergillus* RabB^{Rab5} integrates acquisition of degradative identity with the long-distance movement of early endosomes. *Mol. Biol. Cell* 21, 2756–2769. <https://doi.org/10.1091/mbc.E10-02-0119>.
- Bergs, A., Ishitsuka, Y., Evangelinos, M., Nienhaus, G.U., and Takeshita, N. (2016). Dynamics of actin cables in polarized growth of the filamentous fungus *Aspergillus nidulans*. *Front. Microbiol.* 7, 682. <https://doi.org/10.3389/fmicb.2016.00682>.
- Bielska, E., Schuster, M., Roger, Y., Berepiki, A., Soanes, D.M., Talbot, N.J., and Steinberg, G. (2014). Hook is an adapter that coordinates kinesin-3 and dynein cargo attachment on early endosomes. *J. Cell Biol.* 204, 989–1007. 4481. <https://doi.org/10.1083/jcb.201309022>.
- Burke, J.E., Inglis, A.J., Perisic, O., Masson, G.R., McLaughlin, S.H., Rutaganira, F., Shokat, K.M., and Williams, R.L. (2014). Structures of PI4KIIIβ complexes show simultaneous recruitment of Rab11 and its effectors. *Science* 344, 1035–1038. <https://doi.org/10.1126/science.1253397>.
- Cole, J.L. (2004). Analysis of heterogeneous interactions. *Methods Enzymol.* 384, 212–232. [https://doi.org/10.1016/S0076-6879\(04\)84013-8](https://doi.org/10.1016/S0076-6879(04)84013-8).
- Cove, D.J. (1966). The induction and repression of nitrate reductase in the fungus *Aspergillus nidulans*. *Aspergillus nidulans Biochim Biophys Acta* 113, 51–56. [https://doi.org/10.1016/S0926-6593\(66\)80120-0](https://doi.org/10.1016/S0926-6593(66)80120-0).
- Cross, J.A., and Dodding, M.P. (2019). Motor-cargo adaptors at the organelle–cytoskeleton interface. *Curr. Opin. Cell Biol.* 59, 16–23. <https://doi.org/10.1016/j.ceb.2019.02.010>.
- Donovan, K.W., and Bretscher, A. (2015a). Head-to-tail regulation is critical for the *in vivo* function of myosin V. *J. Cell Biol.* 209, 359–365. <https://doi.org/10.1083/jcb.201411010>.
- Donovan, K.W., and Bretscher, A. (2015b). Tracking individual secretory vesicles during exocytosis reveals an ordered and regulated process. *J. Cell Biol.* 210, 181–189. <https://doi.org/10.1083/jcb.201501118>.
- Goldenring, J.R. (2015). Recycling endosomes. *Curr. Opin. Cell Biol.* 35, 117–122. <https://doi.org/10.1016/j.ceb.2015.04.018>.

- Hales, C.M., Vaerman, J.-P., and Goldenring, J.R. (2002). Rab11 family interacting protein 2 associates with myosin Vb and regulates plasma membrane recycling. *J. Biol. Chem.* 277, 50415–50421. <https://doi.org/10.1074/jbc.M209270200>.
- Hammer, J.A., 3rd, and Sellers, J.R. (2012). Walking to work: roles for class V myosins as cargo transporters. *Nat. Rev. Mol. Cell Biol.* 13, 13–26. <https://doi.org/10.1038/nrm3248>.
- Hernández-González, M., Bravo-Plaza, I., Pinar, M., de los Ríos, V., Arst, H.N., Jr., and Peñalva, M.A. (2018a). Endocytic recycling via the TGN underlies the polarized hyphal mode of life. *PLoS Genet.* 14, e1007291. <https://doi.org/10.1371/journal.pgen.1007291>.
- Hernández-González, M., Pantazopoulou, A., Spanoudakis, D., Seegers, C.L.C., Peñalva, M.A., and Peñalva, M.A. (2018b). Genetic dissection of the secretory route followed by a fungal extracellular glycosyl hydrolase. *Mol. Microbiol.* 109, 781–800. <https://doi.org/10.1111/mmi.14073>.
- Hernández-González, M., Peñalva, M.A., and Pantazopoulou, A. (2014). Conditional inactivation of *Aspergillus nidulans* sarA uncovers the morphogenetic potential of regulating endoplasmic reticulum (ER) exit. *Mol. Microbiol.* 95, 491–508. <https://doi.org/10.1111/mmi.12880>.
- Hodges, A.R., Bookwalter, C.S., Kremntsova, E.B., and Trybus, K.M. (2009). A nonprocessive class V myosin drives cargo processively when a kinesin-related protein is a passenger. *Curr. Biol.* 19, 2121–2125. <https://doi.org/10.1016/j.cub.2009.10.069>.
- Ikebe, C., Konishi, M., Hirata, D., Matsusaka, T., and Toda, T. (2011). Systematic localization study on novel proteins encoded by meiotically up-regulated ORFs in fission yeast. *Biosci. Biotechnol. Biochem.* 75, 2364–2370. <https://doi.org/10.1271/bbb.110558>.
- Jin, Y., Sultana, A., Gandhi, P., Franklin, E., Hamamoto, S., Khan, A.R., Munson, M., Schekman, R., and Weisman, L.S. (2011). Myosin V transports secretory vesicles via a Rab GTPase cascade and interaction with the exocyst complex. *Dev. Cell* 21, 1156–1170. <https://doi.org/10.1016/j.devcel.2011.10.009>.
- Jumper, J., Evans, R., Pritzel, A., Green, T., Figurnov, M., Ronneberger, O., Tunyasuvunakool, K., Bates, R., Zidek, A., Potapenko, A., et al. (2021). Highly accurate protein structure prediction with AlphaFold. *Nature* 596, 583–589. <https://doi.org/10.1038/s41586-021-03819-2>.
- Käll, L., Canterbury, J.D., Weston, J., Noble, W.S., and MacCoss, M.J. (2007). Semi-supervised learning for peptide identification from shotgun proteomics datasets. *Nat. Methods* 4, 923–925. <https://doi.org/10.1038/nmeth1113>.
- Laue, T.M., Shah, B.D., Ridgeway, T.M., and Pelletier, S.L. (1992). Interpretation of analytical sedimentation data for proteins. In *Analytical Ultracentrifugation in Biochemistry and Polymer Science*, S.E. Harding, A.J. Rowe, and J.C. Horton, eds. (Royal Society of Chemistry), pp. 90–125.
- Li, B.X., Satoh, A.K., and Ready, D.F. (2007). Myosin V, Rab11, and dRip11 direct apical secretion and cellular morphogenesis in developing *Drosophila* photoreceptors. *J. Cell Biol.* 177, 659–669. <https://doi.org/10.1083/jcb.200610157>.
- Lipatova, Z., Tokarev, A.A., Jin, Y., Mulholland, J., Weisman, L.S., and Segev, N. (2008). Direct interaction between a myosin V motor and the Rab GTPases Ypt31/32 is required for polarized secretion. *Mol. Biol. Cell* 19, 4177–4187. <https://doi.org/10.1091/mbc.e08-02-0220>.
- Lwin, K.M., Li, D., and Bretscher, A. (2016). Kinesin-related Smy1 enhances the Rab-dependent association of myosin-V with secretory cargo. *Mol. Biol. Cell* 27, 2450–2462. <https://doi.org/10.1091/mbc.E16-03-0185>.
- Matsui, T., Ohbayashi, N., and Fukuda, M. (2012). The Rab interacting lysosomal protein (RILP) homology domain functions as a novel effector domain for small GTPase Rab36: Rab36 regulates retrograde melanosome transport in melanocytes. *J. Biol. Chem.* 287, 28619–28631. <https://doi.org/10.1074/jbc.M112.370544>.
- Mirdita, M., Schütze, K., Moriwaki, Y., Heo, L., Ovchinnikov, S., and Steinegger, M. (2022). ColabFold - making protein folding accessible to all. Preprint at bioRxiv. <https://doi.org/10.1101/2021.08.15.456425>.
- Musacchio, A. (2022). On the role of phase separation in the biogenesis of membraneless compartments. *EMBO J.* 41, e109952. <https://doi.org/10.15252/embj.2021109952>.
- Nayak, T., Szewczyk, E., Oakley, C.E., Osmani, A., Ukil, L., Murray, S.L., Hynes, M.J., Osmani, S.A., and Oakley, B.R. (2006). A versatile and efficient gene-targeting system for *Aspergillus nidulans*. *Genetics* 172, 1557–1566. <https://doi.org/10.1534/genetics.105.052563>.
- Pantazopoulou, A., Pinar, M., Xiang, X., and Peñalva, M.A. (2014). Maturation of late Golgi cisternae into RabE^{RAB11} exocytic post-Golgi carriers visualized *in vivo*. *Mol. Biol. Cell* 25, 2428–2443. <https://doi.org/10.1091/mbc.E14-02-0710>.
- Pashkova, N., Jin, Y., Ramaswamy, S., and Weisman, L.S. (2006). Structural basis for myosin V discrimination between distinct cargoes. *EMBO J.* 25, 693–700. <https://doi.org/10.1038/sj.emboj.7600965>.
- Pearson, C.L., Xu, K., Sharpless, K.E., and Harris, S.D. (2004). MesA, a novel fungal protein required for the stabilization of polarity axes in *Aspergillus nidulans*. *Mol Biol Cell* 15, 3658–3672. <https://doi.org/10.1091/mbc.e03-11-0803>.
- Peñalva, M.A. (2005). Tracing the endocytic pathway of *Aspergillus nidulans* with FM4-64. *Fungal Genet. Biol.* 42, 963–975. <https://doi.org/10.1016/j.fgb.2005.09.004>.
- Peñalva, M.A., Zhang, J., Xiang, X., and Pantazopoulou, A. (2017). Transport of fungal Rab11 secretory vesicles involves myosin-5, dynein/dynactin/p25 and kinesin-1 and is independent of kinesin-3. *Mol. Biol. Cell* 28, 947–961. <https://doi.org/10.1091/mbc.E16-08-0566>.
- Pfeffer, S.R. (2013). Rab GTPase regulation of membrane identity. *Curr. Opin. Cell Biol.* 25, 414–419. <https://doi.org/10.1016/j.ceb.2013.04.002>.
- Pinar, M., Arias-Palomo, E., de los Ríos, V., Arst, H.N., Jr., and Peñalva, M.A. (2019). Characterization of *Aspergillus nidulans* TRAPPs uncovers unprecedented similarities between fungi and metazoans and reveals the modular assembly of TRAPP. *PLoS Genet.* 15, e1008557. <https://doi.org/10.1371/journal.pgen.1008557>.
- Pinar, M., Arst, H.N., Jr., Pantazopoulou, A., Tagua, V.G., de los Ríos, V., Rodríguez-Salarichs, J., Díaz, J.F., and Peñalva, M.A. (2015). TRAPP II regulates exocytic Golgi exit by mediating nucleotide exchange on the Ypt31 ortholog RabE^{RAB11}. *Proc. Natl. Acad. Sci. U S A* 112, 4346–4351. <https://doi.org/10.1073/pnas.1419168112>.
- Pinar, M., Pantazopoulou, A., Arst, H.N., Jr., and Peñalva, M.A. (2013a). Acute inactivation of the *Aspergillus nidulans* Golgi membrane fusion machinery: correlation of apical extension arrest and tip swelling with cisternal disorganization. *Mol. Microbiol.* 89, 228–248. <https://doi.org/10.1111/mmi.12280>.
- Pinar, M., Pantazopoulou, A., and Peñalva, M.A. (2013b). Live-cell imaging of *Aspergillus nidulans* autophagy: Rab1 dependence, Golgi independence and ER involvement. *Autophagy* 9, 1024–1043. <https://doi.org/10.4161/autophagy.24483>.
- Pinar, M., and Peñalva, M.A. (2017). *Aspergillus nidulans* BapH is a Rab11 effector that connects membranes in the Spitzenkörper with basal autophagy. *Mol. Microbiol.* 106, 452–468. <https://doi.org/10.1111/mmi.13777>.
- Pinar, M., and Peñalva, M.A. (2020). *En bloc* TGN recruitment of *Aspergillus* TRAPP II reveals TRAPP maturation as unlikely to drive Rab1-to-Rab11 transition. *J. Cell Sci.* 133, jcs241141. <https://doi.org/10.1242/jcs.241141>.
- Pinar, M., and Peñalva, M.A. (2021). The fungal RABOME: Rab GTPases acting in the endocytic and exocytic pathways of *Aspergillus nidulans* (with excursions to other filamentous fungi). *Mol Microbiol* 116, 53–70, in Press. <https://doi.org/10.1111/mmi.14716>.
- Puerner, C., Serrano, A., Wakade, R.S., Bassilana, M., and Arkowitz, R.A. (2021). A myosin light chain is critical for fungal growth Robustness in *Candida albicans*. *mBio* 12, e0252821. <https://doi.org/10.1128/mBio.02528-21>.
- Pylypenko, O., Attanda, W., Gauquelin, C., Lahmani, M., Coulibaly, D., Baron, B., Hoos, S., Titus, M.A., England, P., and Houdusse, A.M. (2013). Structural basis of myosin V Rab GTPase-dependent cargo recognition. *Proc. Natl. Acad. Sci. U S A* 110, 20443–20448. <https://doi.org/10.1073/pnas.1314329110>.
- Pylypenko, O., Welz, T., Tittel, J., Kollmar, M., Chardon, F., Malherbe, G., Weiss, S., Michel, C.I.L., Samol-Wolf, A., Grasskamp, A.T., et al. (2016). Coordinated recruitment of Spir actin nucleators and myosin V motors to Rab11 vesicle membranes. *Elife* 5, e17523. <https://doi.org/10.7554/eLife.17523>.
- Qiu, R., Zhang, J., and Xiang, X. (2019). LIS1 regulates cargo-adaptor-mediated activation of dynein by overcoming its autoinhibition *in vivo*. *J. Cell Biol.* 218, 3630–3646. <https://doi.org/10.1083/jcb.201905178>.

- Randall, T.S., Yip, Y.Y., Wallock-Richards, D.J., Pfisterer, K., Sanger, A., Fieck, W., Steiner, R.A., Beavil, A.J., Parsons, M., and Dodding, M.P. (2017). A small-molecule activator of kinesin-1 drives remodeling of the microtubule network. *Proc. Natl. Acad. Sci. U S A* **114**, 13738–13743. <https://doi.org/10.1073/pnas.1715115115>.
- Riquelme, M., Bredeweg, E.L., Callejas-Negrete, O., Roberson, R.W., Ludwig, S., Beltrán-Aguilar, A., Seiler, S., Novick, P., and Freitag, M. (2014). The *Neurospora crassa* exocyst complex tethers Spitzenkörper vesicles to the apical plasma membrane during polarized growth. *Mol. Biol. Cell* **25**, 1312–1326. <https://doi.org/10.1091/mbc.E13-06-0299>.
- Roland, J.T., Bryant, D.M., Datta, A., Itzen, A., Mostov, K.E., and Goldenring, J.R. (2011). Rab GTPase–Myo5B complexes control membrane recycling and epithelial polarization. *Proc. Natl. Acad. Sci. U S A* **108**, 2789–2794. <https://doi.org/10.1073/pnas.1010754108>.
- Santiago-Tirado, F.H., Legesse-Miller, A., Schott, D., and Bretscher, A. (2011). PI4P and Rab inputs collaborate in myosin-V-dependent transport of secretory compartments in yeast. *Dev. Cell* **20**, 47–59. <https://doi.org/10.1016/j.devcel.2010.11.006>.
- Schafer, J.C., Baetz, N.W., Lapierre, L.A., McRae, R.E., Roland, J.T., and Goldenring, J.R. (2014). Rab11-FIP2 interaction with MYO5B regulates movement of Rab11a-containing recycling vesicles. *Traffic* **15**, 292–308. <https://doi.org/10.1111/tra.12146>.
- Schuchardt, I., Aßmann, D., Thines, E., Schubert, C., and Steinberg, G. (2005). Myosin-V, Kinesin-1, and Kinesin-3 Cooperate in Hyphal Growth of the Fungus *Ustilago maydis*. *Mol. Biol. Cell* **16**, 5191–5201. <https://doi.org/10.1091/mbc.E05-04-0272>.
- Skolnick, M., Kremontsova, E.B., Warshaw, D.M., and Trybus, K.M. (2013). More than just a cargo adapter, melanophilin prolongs and slows processive runs of myosin Va. *J. Biol. Chem.* **288**, 29313–29322. <https://doi.org/10.1074/jbc.M113.476929>.
- Sharpless, K.E., and Harris, S.D. (2002). Functional characterization and localization of the *Aspergillus nidulans* formin SEPA. *Mol. Biol. Cell* **13**, 469–479. <https://doi.org/10.1091/mbc.01-07-0356>.
- Steinberg, G., Peñalva, M.A., Riquelme, M., Wösten, H.A., and Harris, S.D. (2017). Cell Biology of Hyphal Growth. *Microbiol. Spectr.* **5**. <https://doi.org/10.1128/microbiolspec.FUNK-0034-2016>.
- Szewczyk, E., Nayak, T., Oakley, C.E., Edgerton, H., Xiong, Y., Taheri-Talesh, N., Osmani, S.A., and Oakley, B.R. (2006). Fusion PCR and gene targeting in *Aspergillus nidulans*. *Nat. Protoc.* **1**, 3111–3120. <https://doi.org/10.1038/nprot.2006.405>.
- Taheri-Talesh, N., Horio, T., Araujo-Bazán, L., Dou, X., Espeso, E.A., Peñalva, M.A., Osmani, S.A., and Oakley, B.R. (2008). The tip growth apparatus of *Aspergillus nidulans*. *Mol. Biol. Cell* **19**, 1439–1449. <https://doi.org/10.1091/mbc.E07-05-0464>.
- Taheri-Talesh, N., Xiong, Y., and Oakley, B.R. (2012). The functions of myosin II and myosin V homologs in tip growth and septation in *Aspergillus nidulans*. *PLoS One* **7**, e31218. <https://doi.org/10.1371/journal.pone.0031218>.
- Tilburn, J., Scazzocchio, C., Taylor, G.G., Zabicky-Zissman, J.H., Lockington, R.A., and Davies, R.W. (1983). Transformation by integration in *Aspergillus nidulans*. *Gene* **26**, 205–221. [https://doi.org/10.1016/0378-1119\(83\)90191-9](https://doi.org/10.1016/0378-1119(83)90191-9).
- Todd, R.B., Davis, M.A., and Hynes, M.J. (2007). Genetic manipulation of *Aspergillus nidulans*: heterokaryons and diploids for dominance, complementation and haploidization analyses. *Nat. Protoc.* **2**, 822–830. <https://doi.org/10.1038/nprot.2007.113>.
- Vetter, M., Stehle, R., Basquin, C., and Lorentzen, E. (2015). Structure of Rab11-FIP3-Rabin8 reveals simultaneous binding of FIP3 and Rabin8 effectors to Rab11. *Nat. Struct. Mol. Biol.* **22**, 695–702. <https://doi.org/10.1038/nsmb.3065>.
- Virag, A., and Harris, S.D. (2006). Functional characterization of *Aspergillus nidulans* homologues of *Saccharomyces cerevisiae* Spa2 and Bud6. *Eukaryot. Cell* **5**, 881–895. <https://doi.org/10.1128/EC.00036-06>.
- Wang, Z., Edwards, J.G., Riley, N., Provance, D.W., Karcher, R., Li, X.-d., Davison, I.G., Ikebe, M., Mercer, J.A., Kauer, J.A., and Ehlers, M.D. (2008). Myosin Vb mobilizes recycling endosomes and AMPA receptors for postsynaptic plasticity. *Cell* **135**, 535–548. <https://doi.org/10.1016/j.cell.2008.09.057>.
- Wei, Z., Liu, X., Yu, C., and Zhang, M. (2013). Structural basis of cargo recognitions for class V myosins. *Proc. Natl. Acad. Sci. U S A* **110**, 11314–11319. <https://doi.org/10.1073/pnas.1306768110>.
- Wong, S., Hepowit, N.L., Port, S.A., Yau, R.G., Peng, Y., Azad, N., Habib, A., Harpaz, N., Schuldiner, M., Hughson, F.M., et al. (2020). Cargo release from myosin V Requires the convergence of parallel pathways that phosphorylate and ubiquitylate the cargo adaptor. *Curr. Biol.* **30**, 4399–4412.e7. <https://doi.org/10.1016/j.cub.2020.08.062>.
- Wong, S., and Weisman, L.S. (2021). Roles and regulation of myosin V interaction with cargo. *Adv Biol Regul.* **79**, 100787. <https://doi.org/10.1016/j.jbior.2021.100787>.
- Wu, S.-Z., and Bezanilla, M. (2018). Actin and microtubule cross talk mediates persistent polarized growth. *J. Cell Biol.* **217**, 3531–3544. <https://doi.org/10.1083/jcb.201802039>.
- Wu, X.S., Rao, K., Zhang, H., Wang, F., Sellers, J.R., Matesic, L.E., Copeland, N.G., Jenkins, N.A., and Hammer, J.A., 3rd (2002). Identification of an organelle receptor for myosin-Va. *Nat. Cell Biol.* **4**, 271–278. <https://doi.org/10.1038/ncb760>.
- Wu, X.S., Tsan, G.L., and Hammer, J.A., III (2005). Melanophilin and myosin Va track the microtubule plus end on EB1. *J. Cell Biol.* **171**, 201–207. <https://doi.org/10.1083/jcb.200503028>.
- Yao, X., Wang, X., and Xiang, X. (2014). FHIP and FTS proteins are critical for dynein-mediated transport of early endosomes in *Aspergillus*. *Mol. Biol. Cell* **25**, 2181–2189. <https://doi.org/10.1091/mbc.E14-04-0873>.
- Zhang, J., Qiu, R., Arst, H.N., Jr., Peñalva, M.A., and Xiang, X. (2014). HookA is a novel dynein-early endosome linker critical for cargo movement *in vivo*. *J. Cell Biol.* **204**, 1009–1026. <https://doi.org/10.1083/jcb.201308009>.
- Zhang, J., Tan, K., Wu, X., Chen, G., Sun, J., Reck-Peterson, S.L., Hammer, J.A., 3rd, and Xiang, X. (2011). *Aspergillus* Myosin-v supports polarized growth in the absence of microtubule-based transport. *PLoS One* **6**, e28575. <https://doi.org/10.1371/journal.pone.0028575>.
- Zheng, P., Nguyen, T.A., Wong, J.Y., Lee, M., Nguyen, T.A., Fan, J.S., Yang, D., and Jedd, G. (2020). Spitzenkörper assembly mechanisms reveal conserved features of fungal and metazoan polarity scaffolds. *Nat. Commun.* **11**, 2830. <https://doi.org/10.1038/s41467-020-16712-9>.

STAR★METHODS

KEY RESOURCES TABLE

REAGENT or RESOURCE	SOURCE	IDENTIFIER
Antibodies		
Anti-HA rat mAb	Merck	Cat# 11867423001, RRID:AB_390918
Anti-HIS	Clontech	Cat# 631212, RRID:AB_2721905
Anti-MyoE	This study	Custom made/custom c
Anti-GFP	Merck	Cat# 11814460001, RRID:AB_390913
Anti-Rat Ig, Mouse ads-HRP	Southern Biotechnology	Cat# 3010-05, RRID:AB_2795801
Anti-Mouse IgG (H + L) HRP-conjugated	Jackson ImmunoResearch	Cat# 115-035-003, RRID:AB_10015289
Anti-Rabbit IgG, HRP-linked whole Ab (from donkey)	Cytiva	NA934, RRID:AB_772206v
Chemicals, peptides, and recombinant proteins		
HI-TRAP NHS columns	Cytiva	Cat# 17-0716-01
Glutathione Sepharose 4B	Sigma-Aldrich	Cat# 17-0756-01
nProtein A Sepharose 4 Fast Flow	Cytiva	Cat# 17-5280-01
Ni-Sepharose Hight performance	Sigma-Aldrich	Cat# 17-5268-01
GFP-TRAP magnetic agarose	Chromotek	Cat# gtma-20
PD-10 desalting columns	Cytiva	Cat# 17-0851-01
PD midiTrap G25 columns	Cytiva	Cat# 28918008
HiLoad 16/600 superdex column	Sigma-Aldrich	Cat# GE28-9893-35
GDP	Jena Bioscience	Cat# UN-1172
GTP γ S	Jena Bioscience	Cat# UN-412
Complete, EDTA-free Protease Inhibitor Cocktail	Sigma-Aldrich	Cat# 11873580001
Complete ULTRA Tablets, EDTA-free	Sigma-Aldrich	Cat# 05892953001
Pierce Centrifuge Columns, 0.8 mL	ThermoFisher	Cat# 89869
Clarity Western ECL Substrate	Biorad	Cat#1705061
Critical commercial assays		
TNT SP6 Quick Transcription/Translation System	Promega	Cat# L2080
NucleoBond Xtra Midi columns	Macherey Nagel	Cat# 740412
Experimental models: Organisms/strains		
Please refer to Table S1		N/A
Oligonucleotides		N/A
Please refer to Table S2		N/A
Recombinant DNA		N/A
Plasmid: pET21b	Fisher Scientific	Cat# 69-741-3
Plasmid: pGEX2T	Merck	Cat# GE28-9546-53
Plasmid: pSP64 poly(A)	Promega	Cat# P1241
Plasmid: pET21b-RAB11-GST	This study	N/A
Plasmid: pET21b-Sec4-GST	This study	N/A
Plasmid: pET21b-Rab5b-GST	This study	N/A
Plasmid: pGEX2T-UDS1	This study	N/A
Plasmid: pGEX2T-GTD ^{MyoE}	This study	N/A
Plasmid: pSP64 MyoE	This study	N/A
Plasmid: pSP64 HMSV-HA	This study	N/A

(Continued on next page)

Continued

REAGENT or RESOURCE	SOURCE	IDENTIFIER
Plasmid: pSP64 UsoA-HA	This study	N/A
Plasmid: pET21b-UDS1	This study	N/A
Plasmid: pET21b-RAB11	This study	N/A
Plasmid: pET21b-RAB5b	This study	N/A
Plasmid: pET21b-Sec4	This study	N/A

Software and algorithms

Metamorph	Molecular devices	https://www.moleculardevices.com/products/cellular-imaging-systems/acquisition-and-analysis-software/metamorph-microscopy
Huygens Professional software	Hilversum	https://svi.nl/Homepage
GraphPad Prism 8.02	GraphPad	https://www.graphpad.com/
Image J		https://imagej.nih.gov/ij/
HeteroAnalysis software	(Cole, 2004)	https://biophysics.core.uconn.edu/au-software-and-quicklinks/
SEDNTERP software	(Laue et al., 1992)	N/A
Corel Draw 2020	Corel Corporation	https://www.coreldraw.com/
AlphaFold2	(Jumper et al., 2021)	https://github.com/deepmind/alphafold
ColabFold	(Mirdita et al., 2022)	https://github.com/sokrypton/ColabFold
Mascot search engine version 2.6	Matrix science	https://www.matrixscience.com/
PCOILS	MPI Bioinformatics Toolkit	https://toolkit.tuebingen.mpg.de/tools/pcoils

RESOURCE AVAILABILITY

Lead contact

Further information and requests for reagents should be directed to and will be fulfilled by the Lead Contact: Mario Pinar (mps@cib.csic.es). Department of Cellular and Molecular Biology, Centro de Investigaciones Biológicas Margarita Salas, Ramiro de MAeztu, 9, Madrid, 28040, Spain.

Materials availability

All materials generated in this study are available from the lead contact without restriction.

Data and code availability

- All data central to supporting the main claims of the paper are included with the text. Raw microscopy series will be available from the lead contact, mps@cib.csic.es.
- This paper does not report any original code.
- All additional information required to re-analyze the data reported in this paper is be available from the lead contact, mps@cib.csic.es.

EXPERIMENTAL MODEL AND SUBJECT DETAILS

Aspergillus techniques

Standard A. *nidulans* media were used for strain propagation and conidiospore production (Cove, 1966). GFP and epitope-tagged alleles were introduced in the different genetic backgrounds by meiotic recombination (Todd et al., 2007) and/or transformation (Tilburn et al., 1983), which used recipient *nkuAΔ* strains deficient in the non-homologous end joining pathway (Nayak et al., 2005). Complete strain genotypes are listed in Table S1.

Null mutant strains and protein tagging

uds1Δ, *hmsVΔ*, *sec4Δ* (Pantazopoulou et al., 2014) and *myoEΔ* (Taheri-Talesh et al., 2012) were constructed by transformation-mediated gene replacement with cassettes made by fusion PCR carrying appropriate selectable markers (Szewczyk et al., 2006). Integration events were confirmed by PCR with external primers.

The following proteins were C-terminally tagged endogenously, using cassettes constructed by fusion PCR (Nayak et al., 2005; Szweczyk et al., 2006): UDS1-GFP, UDS1-HA3, UDS1-tdTomato, HMSV-GFP, HMSV-HA3, MyoE-GFP (Taheri-Talesh et al., 2012), MyoE-mCherry and ChsB-GFP (Hernández-González et al., 2018a). GFP-RAB11 (Pantazopoulou et al., 2014) and mCherry-RAB11 (Pinar and Peñalva, 2020) were expressed from its own promoter. Primers used in strain construction are listed in Table S2.

METHOD DETAILS

GFP-MyoE GTD and GFP-MyoE ΔGTD transgenes driven by the *inuA* promoter

GFP-MyoE GTD

A transforming cassette consisting of, from 5' to 3', the sucrose-inducible promoter of the inulinase gene (*inuA*) (Hernández-González et al., 2018b), the GFP-coding sequence translationally fused to the coding sequence for residues 1082 through 1569 of MyoE, the *Aspergillus fumigatus* *pyrG* gene and the *inuA* gene 3'-flanking region was constructed by 5-way fusion PCR (Taheri-Talesh et al., 2008), using the following primers (underlined sequences indicate regions of overlap used for fusion PCRs):

(1) : *inuA* promoter region, PCR-amplified with primers:

5'-GTGGAGGCCACTCTCGGAAAC-3'

5'-CAGTGAAAAGTTCTTCTCCTTACTCATTTTGGTGATGTCGCTGACCGC-3'

(the underlined overlapped with GFP-coding region)

(2) : GFP-(Gly-Ala)₆

5'-ATGAGTAAAGGAGAAGAAGACTTTTC-3'

5'-GGCACCGGCTCCAGCGCCTGC-3'

(3) : MyoE-GTD

5'-CTGGTGCAGGCGCTGGAGCCGGTGCCCAGGCGTTGAACGGAGACCAGC-3': [the underlined overlapping with the GFP-(Gly-Ala)₆ coding region.

5'-ATTCCAGCACACTGGCGGCCGTTACTTACTCCATCACCCATTCTCAG-3': (the underlined overlapping with *pyrGAf*)

(4) : *pyrGAf*

5'-GTAACGGCCGCCAGTGTGCTG-3'

5'-GTCTGAGAGGAGGCACTGATG-3'

(5) : *inuA* 3'-UTR

5'-ACGCATCAGTGCCTCCTCTCAGACAGGATCTAGCTAGATGTTTTGTTG-3':

5'-CAGCAGTCAAGCAATACCAAGC-3'

(the underlined overlapping with *pyrGAf*).

GFP-MyoE ΔGTD

Constructed as above, but using as primers (3) to amplify the coding sequence for residues 1-1081 of MyoE the following oligonucleotides:

5'-CTGGTGCAGGCGCTGGAGCCGGTGCCGCGCATAATTATGAGGTCGGGAC-3'

[the underlined overlapping with the GFP-(Gly-Ala)₆ coding region.

5'-ATTCCAGCACACTGGCGGCCGTTACTTAAAGGGGTAATGTCCTCTTTGCG-3':

(the underlined overlapping with pyrGAf).

The cassettes were used to replace the *inuA* gene, considered to be a safe haven, by homologous recombination. *inuAΔ* does not affect growth on carbon sources other than inulin (glucose is used as standard carbon source in *A. nidulans* media). The *inuA^P* is inducible by sucrose, and results in moderate levels of expression (Hernández-González et al., 2018b)

Plasmids for protein expression

GST constructs

pET21b-RAB11-GST: carries cDNA encoding cysteine-less RAB11 with GST C-terminally attached. *NdeI/BamHI* insert in pET21b.

pET21b- Sec4-GST: carries cDNA encoding cysteine-less Sec4 with GST C-terminally attached. *NdeI/XhoI* insert in pET21b.

pET21b-RAB5b-GST: carries cDNA encoding cysteine-less RAB5b with GST C-terminally attached. *NheI/NotI* insert in pET21b.

Note that in all three constructs GST is attached to the C-termini of the RABs, and that they all include a stop codon after the GST coding region to interrupt translation before the His tag.

pGEX2T-GFP: pGEX-2T derivative encoding a GST-sGFP fusion as a *BamHI-EcoRI*.

pGEX2T-UDS1: UDS1 cDNA cloned as *BamHI* in pGEX-2T (N-terminal GST).

pGEX2T-GTD^{MyoE} includes coding sequence for residues 1082 through 1569 (the C-terminus) of MyoE, cloned in phase with GST as *BamHI-XmaI*.

TNT expression constructs

pSP64 MyoE: MyoE cDNA cloned as a *BamHI* fragment in Promega's #P1241 pSP64 poly (A).

pSP64 HMSV-HA: C-terminally HA3-tagged cDNA encoding HMSV cloned as *PstI/XmaI* in pSP64 poly (A).

pSP64 Uso1-HA: C-terminally HA3-tagged cDNA encoding Uso1 cloned as *PstI/XmaI* in pSP64 poly (A).

His6-tagged constructs

pET21b-UDS1: UDS1 cDNA, cloned as *NheI/NotI* in pET21b.

pET21b-RAB11: RAB11 cDNA sequence without the two C-terminal Cys residues, cloned as *NdeI/XhoI* in pET21b.

pET21b-RAB5b: Rab5b cDNA sequence without the two C-terminal Cys residues, cloned as *NheI/XhoI* in pET21b.

pET21b-Sec4: Sec4 cDNA sequence without the two C-terminal Cys residues, cloned as *NdeI/XhoI* in pET21b.

In vitro transcription/translation

Proteins were synthesized using TNT® SP6 Quick Coupled Transcription/Translation system (Promega #L2080) using the standard reaction mix (rabbit reticulocyte lysate plus amino acids) supplemented with 20 μM methionine. Reactions were primed with 1 μg of purified, circular pSP64 derivatives, which were purified using NucleoBond Xtra-Midi columns (Macherey Nagel, #740412).

Antibodies and western blotting

Antisera against MyoE and Uso1 were raised in rabbits by Davids Biotechnology (<https://www.davids-bio.com>). Animals were immunized with His6-tagged polypeptides containing residues 1082-1569 of MyoE (the GTD) or residues 1-659 of USO1. These polypeptides were purified by Ni²⁺ affinity chromatography after expression in *E. coli* BLB21 as described (Pinar et al., 2015). Antibodies against the target proteins were purified from raw antisera (40 mL) by affinity chromatography with the respective antigens, previously coupled to 1 mL HI-TRAP NHS columns (Cytiva #17-0716-01) packed with Sepharose pre-activated for covalent coupling of ligands containing primary amino groups, following instructions of the manufacturer. Antibodies were eluted with 100 mM glycine, pH 3.0, neutralized with 2M Tris, pH 7.5 and stored at –20°C.

Western blots were reacted with the following antibodies

For HA3-tagged proteins

α -HA rat mAb (1/1,000) (Merck #11867423001) as primary antibody, and HRP-conjugated α -rat IgM+IgG, as secondary antibodies (Southern Biotechnology #3010-05; 1:4,000).

For His6-tagged UDS1 and RABs

α -His primary antibody (1/10,000; Clontech #631212) and HRP-conjugated goat anti-mouse IgG (H + L) secondary antibodies (Jackson ImmunoResearch #115-035-003, 1/5000).

For MyoE: MyoE was detected with a custom-made α -MyoE-GTD antiserum (1/4000; see above) and donkey HRP-coupled α -rabbit IgG (Cytiva NA-934) as secondary antibodies.

For α -GFP western blotting

we used Merck #11814460001 mixture of two mouse mAbs (1/5000) as primary antibodies and HRP-conjugated AffiniPure goat anti-mouse IgG (H + L) secondary antibodies (Jackson ImmunoResearch #115-035-003, 1/5000). In all cases reacting bands were detected with Clarity western ECL substrate (Biorad Laboratories #1705061).

RAB-GST purification and nucleotide loading

500 mL bacterial cultures in LB plus antibiotics as appropriate were incubated at 37°C until reaching a O.D. of 0.6–0.8 at 600 nm. These primary cultures were induced with 0.1 mM IPTG, transferred to a 15°C incubator and shaken for an additional 20 h. Cells were collected by centrifugation and stored at –80°C. A pellet corresponding to 250 mL of the culture was resuspended in PBS containing cOmplete™ protease inhibitor cocktail (Sigma-Aldrich #11873580001), 0.2 mg/mL lysozyme and 1 μ g/mL of DNase I (Abenza et al., 2010) and lysed in a French Press. After centrifugation at 30,000 \times g and 4°C for 30 min, the supernatant was mixed with 300 μ L of glutathione Sepharose 4B (Sigma-Aldrich #17-0756-01) and incubated at 4°C for 1 h in a rotating wheel. Sepharose-bound RABs were resuspended in a buffer consisting of 25 mM HEPES PH 7.5, 110 mM KCl, 1 mM DTT, 10 mM EDTA and 125 μ M GDP or GTP γ S and incubated for 30 min at 30°C with gentle rocking. Beads were then washed twice with nucleotide loading buffer (as above, but containing 10 mM Cl₂Mg instead of 10 mM EDTA) before incubating them overnight at 25°C with gentle rocking in nucleotide loading buffer containing GDP or GTP γ S (Jena Bioscience UN-1172 and UN-412, respectively).

UDS1-His6 expression and purification from bacteria

E. coli cells (BLB21 pRIL) carrying pET21b-UDS1 were cultured at 37°C in LB containing ampicillin and chloramphenicol until reaching an OD⁶⁶⁰ of 0.5. At this point cultures were induced with 0.1 M IPTG, transferred to 15°C and incubated overnight before collecting cells by centrifugation and storing pellets at –80°C. Bacterial pellets were thawed, resuspended in 25 mL of lysis buffer (as for RAB-GST proteins), incubated for 30 min in ice, and lysed with a French Press. Lysates were clarified by centrifugation (30,000 \times at 4°C for 30 min) and purified in a Ni-Sepharose High Performance column (Sigma-Aldrich #17-5268-01). Imidazole (0.5 M) present in the eluted fraction was removed with a PD-10 desalting columns (Cytiva #17-0851-01) equilibrated in PBS, pH 7.4 containing 5% glycerol and 1 mM DTT. The eluate (3.5 mL) was loaded onto a HiLoad 16/600 Superdex column (Sigma-Aldrich #GE28-9893-35) that was run at 1 mL/min. Fractions containing protein were analyzed by SDS-PAGE, stained with Coomassie and pooled as appropriate.

RAB-His6 purification and nucleotide loading

Expression and Ni²⁺ Sepharose affinity purification were carried out as above. Imidazole was removed with PD midiTrap G25 columns (Cytiva #28918008) in 75 mM HEPES, pH 7.5, 150 mM KCl and 1 mM DTT. Eluted RABs were incubated with 1 mM GDP or GTPγS and 10 mM EDTA for 30 min at 30°C. Then, 20 mM MgCl₂ was added, and the solutions were aliquoted, flash-frozen and stored at -80°C.

Total cell extracts

These were carried out as described (Pinar et al., 2019). 70 mg of lyophilized mycelia were ground to a fine powder in 2 mL tubes containing a ceramic bead and a 20 s pulse of a FastPrep set at power 4. The powder was suspended in 1.5 mL of 'low KCl buffer' (25 mM HEPES, pH 7.5, 110 mM KCl, 5 mM MgCl₂, 1 mM DTT and 0.1% Triton) containing 10% (v/v) glycerol, complete ULTRA Tablets inhibitor cocktail (Sigma-Aldrich #05892953001) and ~ 100 μL of 0.6 mm glass beads. The resulting suspension was homogenized with a 15 s full-power pulse of the FastPrep and proteins were extracted after incubation for 10 min at 4°C in a rotating wheel. This extraction step was repeated two additional times before the resulting homogenate was clarified by centrifugation at 15,000 × g and 4°C in a refrigerated microcentrifuge.

RAB-GST pull-downs with total cell extracts

6 mg of each extract were mixed with 10 μL of nucleotide-loaded RAB-GST baits in a total volume of 0.4 mL in 0.8 mL Pierce centrifuge columns (ThermoFisher #89869) and the mixtures were incubated for 2 h at 4°C in a rotating wheel. GST-Sepharose beads were collected by low speed centrifugation, washed four times with 0.7 mL of 'medium KCl buffer' (25 mM HEPES pH 7.5, 175 mM KCl, 5 mM MgCl₂, 1 mM DTT and 0.1% Triton X-100) before bound material was eluted with 20 μL of Laemmli loading buffer. 15 μL were run in 7.5% polyacrylamide gels that were analyzed by α-HA western blotting and 2 μL were run in a 10% polyacrylamide gel for Coomassie staining of the baits.

RAB-GST pull-downs with purified proteins

Binding reactions were carried out in 0.8 mL Pierce centrifuge columns. Nucleotide-loaded RABs (10 μL of glutathione Sepharose beads) were mixed with either 2.5 μg of purified UDS1-His6 or with 10 μL of TNT reaction mix primed with appropriate plasmids (pSP64-MyoE, pSP64-HMSV-HA3 or pS64-Uso1-HA3), in 0.4 mL of 'medium KCl' buffer containing 10% glycerol. The resulting mix was incubated for 2 h at 4°C in a rotating wheel. Beads were collected by low-speed microcentrifugation and washed four times in the same buffer before eluting bound material with 20 μL of Laemmli loading buffer. 5 μL aliquots were analyzed by western blotting using α-His antibody (for UDS1-His6) or α-HA antibody (for HMSV-HA3) and 7.5% polyacrylamide gels, or α-MyoE antibodies and Biorad's pre-casted 4–15% polyacrylamide gels (for MyoE).

Pull-down of the UDS1-HMSV complex with RAB11-GST

10 μL of glutathione Sepharose beads loaded with RAB11-GST GTPγS or GDP were incubated in Pierce microcolumns for 2 h at 4°C with 2.5 μg of UDS1-His6 and 10 μL of TNT-synthesized HMSV-HA3 in 400 μL of 'low KCl' buffer containing 10% glycerol. Beads were washed four times with 'medium KCl' buffer. Equal amounts of bound material were analyzed by western blotting using α-HA3 and α-His antibodies.

Pull-down experiments of TNT-expressed proteins with GST fusion protein baits

GST-UDS1, GST-GTD and GST-GFP baits were purified as described for RAB-GST proteins. 15 μL of glutathione Sepharose beads containing bait protein fusions were mixed with 10 μL of TNT-synthesized HMSV-HA3 or Uso1-HA3 preys (10 μL of each reaction mix) in 0.4 mL of 25 mM HEPES pH 7.5, 300 mM KCl, 0.5% Triton, 0.5 mM EDTA and 1 mM DTT, using Pierce microcolumns, which were incubated for 2 h at 4°C in a rotating wheel. Beads were washed four times with the same buffer and eluted with 20 μL of Laemmli buffer. 5 μL aliquots were analyzed by α-HA western blotting.

Pull-down experiments of RAB preys with GST-GTD

Sepharose beads (10 μL slurry) loaded with either GST-GTD or, as negative control, GST-GFP fusion proteins were mixed with the different RABs (final concentration 50 nM) in 50 mM HEPES pH 7.5, 110 mM KCl, 5 mM MgCl₂, 0.1% Triton X-100 (v/v) and 10% (v/v) glycerol (500 μL final volume) in 0.8 mL Pierce microcolumns. The reaction mixtures were rotated overnight at 4°C before beads were recovered by centrifugation and washed four times in 50 mM HEPES pH 7.5, 250 mM KCl, 5 mM MgCl₂ and 0.1% Triton X-100 (v/v) for

10 min at 4°C. Bound proteins were eluted with 20 μ L of Laemmli loading buffer. 15 μ L samples were analyzed by α -His western blotting using 12% polyacrylamide gels. A gel run in parallel was stained with Coomassie blue to assess equal loading of GST baits.

ProtA immunoprecipitations

For α -MyoE co-immunoprecipitation experiments of HMSV-HA3, 5 μ L samples of Protein A-Sepharose (Cytiva #17-5280-01) were preincubated with 10 μ L each of purified α -MyoE or α -Uso1 antibodies for 3 h at room temperature. Antibody-loaded beads were mixed with 25 μ L of TNT-synthesized MyoE and 25 μ L of TNT-synthesized HMSV-HA3 in 0.4 mL of 25 mM HEPES pH 7.5, 500 mM NaCl, 0.5% Triton, 0.5 mM EDTA and 2% BSA, using 0.8 mL Pierce microcolumns. Beads were recovered by microcentrifugation, washed four times in the same buffer (without BSA) and eluted with 20 μ L of Laemmli loading buffer. 5 μ L of each sample were analyzed by western blot (7.5% polyacrylamide gel) using α -HA mAb. A gel run in parallel was stained with Coomassie blue to assess equal loading of Protein A beads with IgG heavy chains.

GFP-trap and western blotting

Cell extracts [strains, MyoE-GFP (MAD4406), UDS1-GFP (MAD6379), HMSV-GFP (MAD7326) and Uso1-GFP (MAD6358)] were prepared as described above, but using the lysis buffer recommended by the manufacturer, which containing 25 mM Tris-HCl pH 7.5, 150 mM NaCl, 0.5 mM EDTA, 0.5% NP40 and cOmplete protease inhibitors. Approximately 100 mg of total protein (4 mL of extract) were immunoprecipitated with 25 μ L of GFP-Trap magnetic agarose beads (Chromotek #gtma-20) following incubation for 2 h at 4°C in a rotating wheel. Beads were washed four times with the same buffer before eluting the immunoprecipitated material with 60 μ L of Laemmli buffer. 10 μ L aliquots were analyzed by α -HA3 western blotting (7.5% polyacrylamide gels) or α -MyoE western blotting. 2 μ L were analyzed by α -GFP western blotting to determine levels of immunoprecipitated baits. Lastly 8 μ L were analyzed by SDS-PAGE and silver staining. GFP-trap co-immunoprecipitation experiments of HMSV-HA3 with GFP-MyoE [GTD] and MyoE [Δ GTD] were carried out with otherwise *myoE* Δ strains MAD7864 and MAD7862, respectively.

Shotgun proteomic analysis of RAB11-GST effectors

Large scale purification of proteins interacting with the GDP and GTP γ S forms of RAB11-GST was carried out as described previously for GST-RAB11 (Pinar and Peñalva, 2017).

Bound proteins were loaded onto a 10% polyacrylamide gel, which was run until proteins moved 1 cm into the gel. The protein mixture band was detected by colloidal Coomassie staining, excised and processed for tryptic digestion and subsequent analysis by MS/MS essentially as described (Pinar et al., 2019). For MS/MS analyses of GFP-tagged bait associates, proteins were digested using the 'on-bead digest protocol for mass spectrometry following immunoprecipitation with Nano-Traps' recommended by Chromotek. In both cases mass spectra *.raw files were used to search the *A. nidulans* FGSC A4 version_s10m02-r03_orf_trans_all-MOD1 proteome database (8,223 protein entries) using Mascot search engine version 2.6 (Matrix Science). Peptides were filtered using Percolator (Kall et al., 2007), with a q-value threshold set to 0.01.

Analytical ultracentrifugation

Sedimentation equilibrium analysis of UDS1-His was carried out in the Molecular Interactions Facility of the Centro de Investigaciones Biológicas using an XL-A analytical ultracentrifuge (Beckman-Coulter Inc.) equipped with a UV-VIS detector set at 237 nm. Centrifugation was carried out in short (95 μ L) columns at speeds ranging from 6,000 to 9000 rpm, with a last high-speed (48,000 rpm) run to deplete the protein from the meniscus and obtain the corresponding baseline offsets. Weight-average buoyant molecular weights were determined by fitting, using HeteroAnalysis software (Cole, 2004), a single-species model to the experimental data (corrected for temperature and solvent composition with SEDNTERP software (Laue et al., 1992).

Negative staining electron microscopy

Purified UDS1 was diluted to 0.2 μ M in 150 mM NaCl, 25 mM HEPES pH 7.5 and 5% glycerol, and stained with 2% (w/v) uranyl acetate. Specimens were examined under a JEOL 1230 electron microscope equipped with a TVIPS CMOS 4kx4k camera and operated at 100 kV. Data were collected at a nominal magnification of 40,000 \times , which corresponds to 2.84 \AA /pixel at the micrograph level. The length of 71 representative particles selected from multiple micrographs was measured using ImageJ (<https://imagej.nih.gov/ij/>).

Fluorescence microscopy

Hyphae were cultured in watch minimal medium (WMM) (Peñalva, 2005). Microscopy chambers, hardware, software and image acquisition procedures have been thoroughly documented (Pinar and Peñalva, 2020), with the sole exception that some of the experiments using the Hamamatsu Gemini beam splitter were carried out in a Leica DMI8 inverted microscope instead of a Leica DMI6000. Z-stacks were deconvolved using Huygens Professional software (Hilversum, Holland), version 20.04.0p5 64 bits. Images (usually MIPs unless otherwise indicated) were contrasted with Metamorph (Molecular Devices) and annotated using Corel Draw. Movies were assembled with Metamorph and compressed using QuickTime (Apple Inc.). Quantitation of average MyoE-GFP signals in the SPK was made using MIPs of raw images. Datasets were analyzed with GraphPad Prism 7.03 (GraphPad).

To estimate the areas occupied by the RAB11 cluster in wild-type and *sec4Δ* cells (Figure 1D), regions were automatically drawn after thresholding the image and the areas were calculated with Metamorph. A similar procedure was used to determine total intensities of MyoE-GFP in the wild-type and *sec4Δ* SPKs (Figure 1E). Linescans of hyphal tips used for Figure 1I correspond to average values of 3 px-wide ROIs. To determine the widths of wild-type and mutant cells, hyphae were cultured overnight as above before adding calcofluor at 1 μg/mL to label cell walls. Fluorescence pictures (middle planes or, for 3D reconstructions of the septae, z-stacks; 100× magnification optics, 1 px = 0.06 μm) were taken and used to draw linescans perpendicular to the growth axis, which were used to measure the distances between the two sharp peaks corresponding to intersections with the cell wall.

Alpha-Fold predictions

The UDS1 and HSMV AlphaFold2 (Jumper et al., 2021) predictions were run using versions of the program installed locally and on Colab-Fold (Mirdita et al., 2022) with the MMseqs2 MSA option. The input UDS1 sequence (AN5595, 941 residues) was submitted as two separate chains (using a 1:1 homo-oligomer setting) guided by the experimental characterization of the protein.

QUANTIFICATION AND STATISTICAL ANALYSIS

Details are described in the legends to Figures 1, 4 and 7. Analysis was carried out with GraphPad Prism software (v. 7.03).